GEOLOGICA BELGICA ((2014) 17/3-4: 252-267

Regional significance of non-cylindrical folding in the northwestern part of the High-Ardenne slate belt (Redu-Daverdisse, Belgium)

Dominique JACQUES*, Tine DEREZ, Philippe MUCHEZ & Manuel SINTUBIN

Geodynamics and Geofluids Research Group, Department of Earth and Environmental Sciences, KU Leuven, Celestijnenlaan 200E box 2410, B-3001 Leuven.
** corresponding author: dominique.jacques@ees.kuleuven.be*

ABSTRACT. Regional mapping and a detailed geometric analysis of complex, mixed brittle-ductile, fold-related accommodation structures, along the well-exposed banks of the Lesse river between Redu and Daverdisse (Belgium), reveal that the finite strain in the predominantly incompetent Lower Devonian rock sequence in the northwestern part of the High-Ardenne slate belt deviates from pure flattening and approximates plane strain. This finite strain is materialised by different manifestations of non-cylindrical folding, i.e. regional en-echelon and periclinal fold geometries, mesoscale non-cylindrical folds with hinges showing variable plunges, oblique flexural slip and locally a non-axial planar, transecting cleavage. The observed non-cylindrical folding fits in the regional framework of the Meuse Valley Recess, a transpressional corridor in the Ardenne allochthon that developed on top of a buried, buttressing oblique ramp in the pre-structural basement. Differential propagation in the overriding Ardenne allochthonuous domain to the east and west of this buttressing oblique ramp led to a component of lateral shortening on top of the ramp, resulting in the rotation of the overall structural grain and the development of en-echelon, non-cylindrical folds. Our study suggests that the Meuse Valley Recess can be continued towards the southeast, at least affecting the northern parts of the High-Ardenne slate belt.

KEYWORDS. En-echelon periclinal folds; non-axial planar, transecting cleavage; oblique flexural slip; plane strain; sediment architecture; Meuse Valley Recess

1. Introduction

The High-Ardenne slate belt (HASB) is part of the Variscan foreland fold-and-thrust belt, exposed in the Ardenne-Eifel area (Belgium, France, Germany). Previous studies of Variscan deformation in the HASB have focused predominantly on structures related to the contraction-dominated deformation of the incompetent rock, and the resulting strongly anisotropic fabric, e.g. anomalies in the slaty cleavage fabric (e.g. Robion et al., 1999), mullion structures (formerly described as 'boudins') (e.g. Jongmans & Cosgrove, 1993; Kenis & Sintubin, 2007; Lambert & Bellière, 1976; Urai et al., 2001), kink bands (e.g. Fourmarier, 1966; Rondeel, 1971; Van Baelen, 2010), overprinting tectonic foliations (e.g. Piessens & Sintubin, 1997; Schavemaker et al., 2012), foliation boudins (e.g. Van Baelen, 2010), and ductile shear zones (e.g. Schavemaker et al., 2012). Few studies, however, have focused in particular on the folding kinematics of the Variscan deformation (e.g. Lacquement, 2001).

Throughout most of the literature, the folding in the Ardenne allochthon has been regarded as consistently reflecting pure flattening finite strain, characterised by cylindrical folds with an axial planar cleavage. Within the HASB, this cylindrical fold geometry is described as consisting of upright to overturned, north-verging folds with a south-dipping slaty cleavage (Mansy & Lacquement, 2002). The Ardenne culmination, moreover, is mentioned to have a consistent NE-SW structural grain with gently NE-plunging folds (Asselberghs, 1946; Beugnies, 1986). A number of studies, performed in the more competent sequences of the Dinant fold-and-thrust belt, however, indicate that certain zones within the Ardenne allochthon show variations in the structural grain with more curvilinear fold geometries (Hance

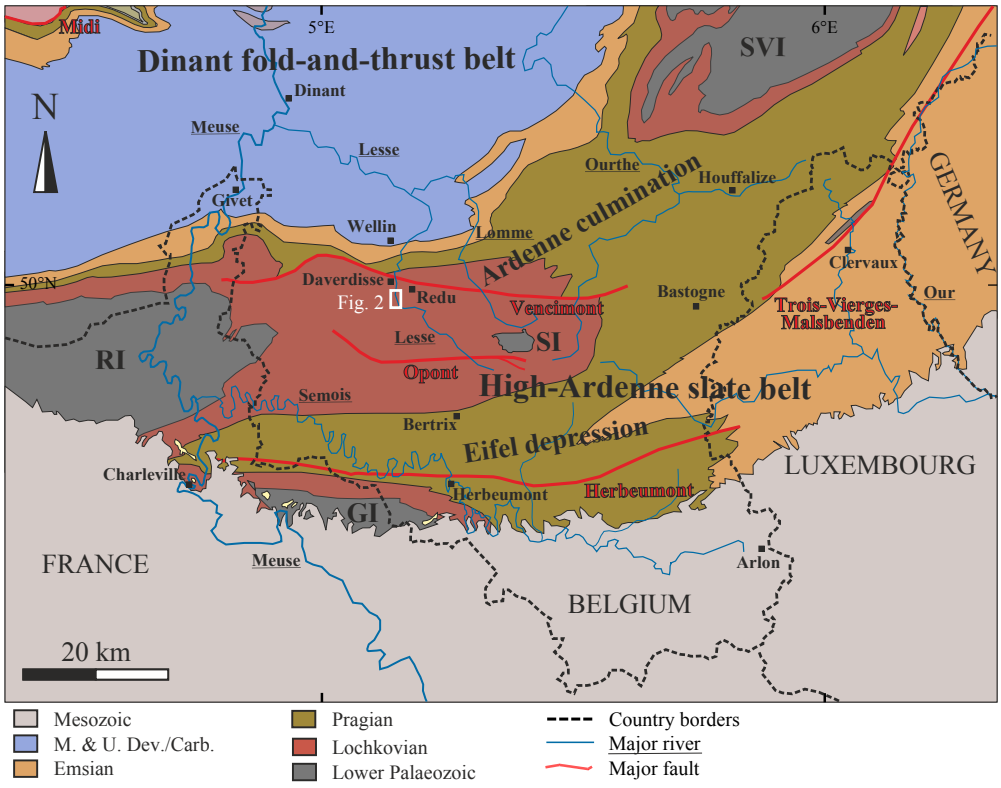

Figure 1. Geological map of the Ardenne-Eifel area with the main tectonostratigraphical units (after Asselberghs, 1946). White rectangle indicates the Redu-Daverdisse study area. RI, SVI, SI, GI: Rocroi, Stavelot-Venn, Serpont and Givonne basement inliers, respectively.

et al., 1999; Lacquement et al., 2005). Additionally, cylindrical folding in general seems more of an exception than the norm (e.g. Lisle et al., 2010).

In this study we demonstrate that the basic assumption of the overall cylindrical nature of folds within the HASB cannot be inferred solely based on individual observations, but that a detailed geometric analysis of regional and mesoscale fold structures is necessary to correctly assess fold geometries. To demonstrate this, we selected a series of brittle to ductile accommodation structures related to the main Variscan folding stage in the well-exposed valley of the Lesse river between the villages of Redu and Daverdisse. This area is part of the heterogeneous Lower Devonian sequence of the northern part of the HASB, just north of the backbone of the Ardenne culmination (Fig. 1). Along the NW-SE trending, previously unstudied section of about 2.5 km (Fig. 2), a number of key exposures were defined. These exposures allow to demonstrate that non-cylindrical folding occurred on a local scale in the northwestern part of the HASB. Moreover, these observations can be fitted within a regional geodynamic framework, suggesting the continuation of a transpressional corridor with curvilinear fold geometries, i.e. the Meuse Valley Recess, recognised in the Dinant fold-and-thrust belt by Lacquement et al. (2005), towards the southeast, affecting at least the northern part of the HASB.

Throughout the text, planar data are presented as dip direction/dip in the azimuth convention, linear data as trend/plunge. The lower-hemisphere equal-area stereographic projections of orientation data are performed with the orientation analysis program OpenStereo 0.1.2 (Grohmann & Campanha, 2010).

2. Geological setting

The Ardenne allochthon is part of the Rhenohercynian foreland fold-and-thrust belt, located at the northern extremity of the Mid-European Variscides (Oncken et al., 1999). It consists primarily of deformed Devono-Carboniferous sediments that were deposited in a shallow marine setting on the northern passive margin of the developing Rhenohercynian ocean (Oncken et al., 1999). The HASB is the southernmost domain of the Ardenne allochthon, exposed in the Ardenne-Eifel area (northern France, Belgium, Luxemburg and western Germany) (Fig. 1). It consists of a thick sequence of predominantly incompetent, metapelitic rocks of early Devonian age, which originated from rapid syn-rift sedimentation in the Ardenne-Eifel basin, particularly active during the Pragian (Oncken et al., 1999). Further to the south, a rift-drift transition occurred during the Emsian (~395Ma), leading to the development of a carbonate platform, now constituting the Dinant fold-and-thrust-belt with competent, well-layered, carbonate sequences. The HASB is further subdivided in the northern Ardenne culmination and the southern Eifel depression. The backbone of the Ardenne culmination consists of several Lower Palaeozoic basement inliers (Rocroi, Serpont, Givonne, and Stavelot-Venn inliers) (Fig. 1).

During the late stages of burial in the early Devonian Ardenne-Eifel basin, the metasediments, now exposed in the HASB, were affected by a very low (anchizonal) to low-grade (epizonal), up to greenschist, metamorphism (Beugnies, 1986; Fielitz & Mansy, 1999). This metamorphism is believed to be pre- to early synkinematic to the Variscan deformation (Fielitz & Mansy, 1999). Basin closure and inversion, occurring during the late Visean to early Namurian, Sudetic stage of the Variscan orogeny (Fielitz & Mansy, 1999; Picqué et al., 1984), resulted in the development of a fold-and-thrust belt. During the latest, Asturian, stage of the Variscan orogeny (late Carboniferous), the Ardenne allochthon was thrusted northwards along the Aachen-Midi fault over its foreland, the Brabant parautochthon (Meilliez & Mansy, 1990). This Lower Palaeozoic basement had previously been deformed by the early Palaeozoic Brabantian orogeny, taking place from the Llandovery-Wenlock to the Eifelian (Debacker et al., 2005; Sintubin et al., 2009).

3. Lithology and sedimentology

The rocks in the study area belong to the Saint-Hubert Formation, Lochkovian/Pragian in age (Bultynck & Dejonghe, 2001). These rocks were deposited in the land-sea transition zone of a siliciclastic delta system, as suggested by Stets & Schäfer (2009) for the Lower Devonian of the Rhenohercynian Basin. The lithology consists of an alternation of dominant greenish to greenish grey metapelites with psammites and minor quartzitic sandstones. The fossil record of the formation is very poor (Asselberghs, 1946).

In the field, metapelites, siltstones and psammites are intercalated with minor centimetre- to metre-scale coarse-grained quartzitic sandstones. In the fine-grained metapelites a cleavage is pervasively developed, internal bedding is mostly difficult to recognise and kink bands occasionally developed (Fig. 3A). Locally, also some oxidised pyrite grains were observed. The fine-grained psammites have a strongly developed internal lamination with a straight to wavy character (Fig. 3B). The psammites locally contain small-scale sand balls (Fig. 3B) and a planar cross-lamination (Fig. 3C). The quartzitic sandstones are very often cross-stratified and range from asymmetric (point) bars (see paragraphs 4.3 & 4.4) to metre-thick cross-laminated layers (Fig. 3D & F) and small-scale gullies (Fig. 3G). The cross-laminated layers can be oppositely dipping and are sometimes coated with thin clay-rich laminae or mud drapes (Fig. 3D). At the base of sandy to quartzitic beds some load casts (Fig. 3F), and other

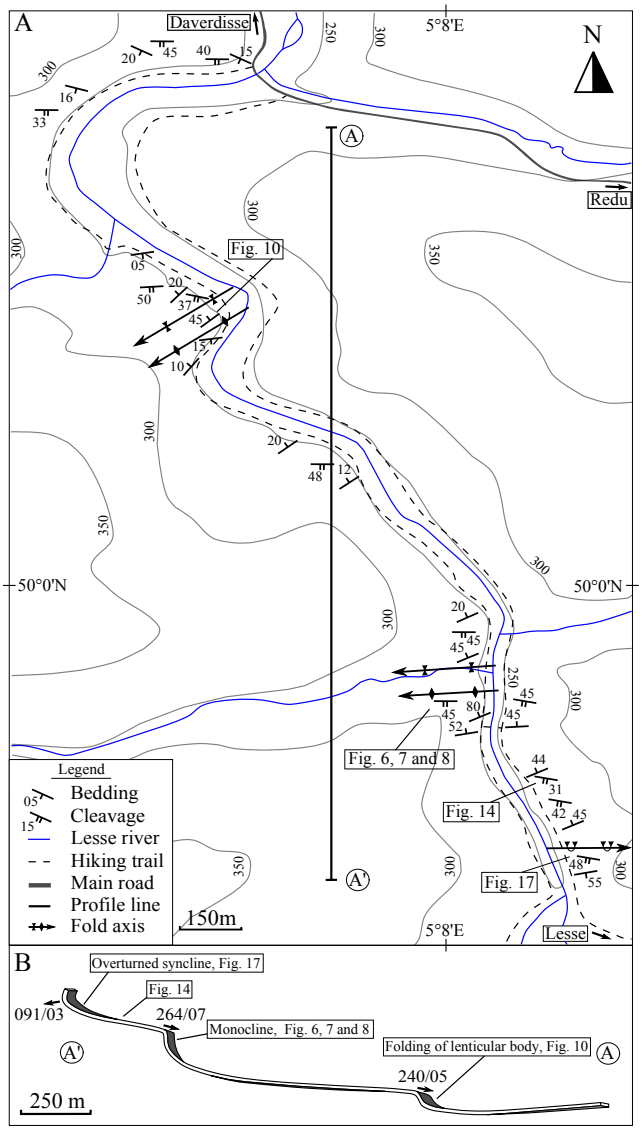

Figure 2. Map (A) and schematic cross-section (B) illustrating the structural architecture in the study area (see Fig. 1 for location). The location of the different exposures and their associated structural data, constraining the fold train, are highlighted. The schematic cross-section (B) is not to scale, but merely intends to illustrate the overall geometry of the fold train (e.g. fold hinge lines). The location of the discussed exposures within the fold train is marked by means of references to figures.

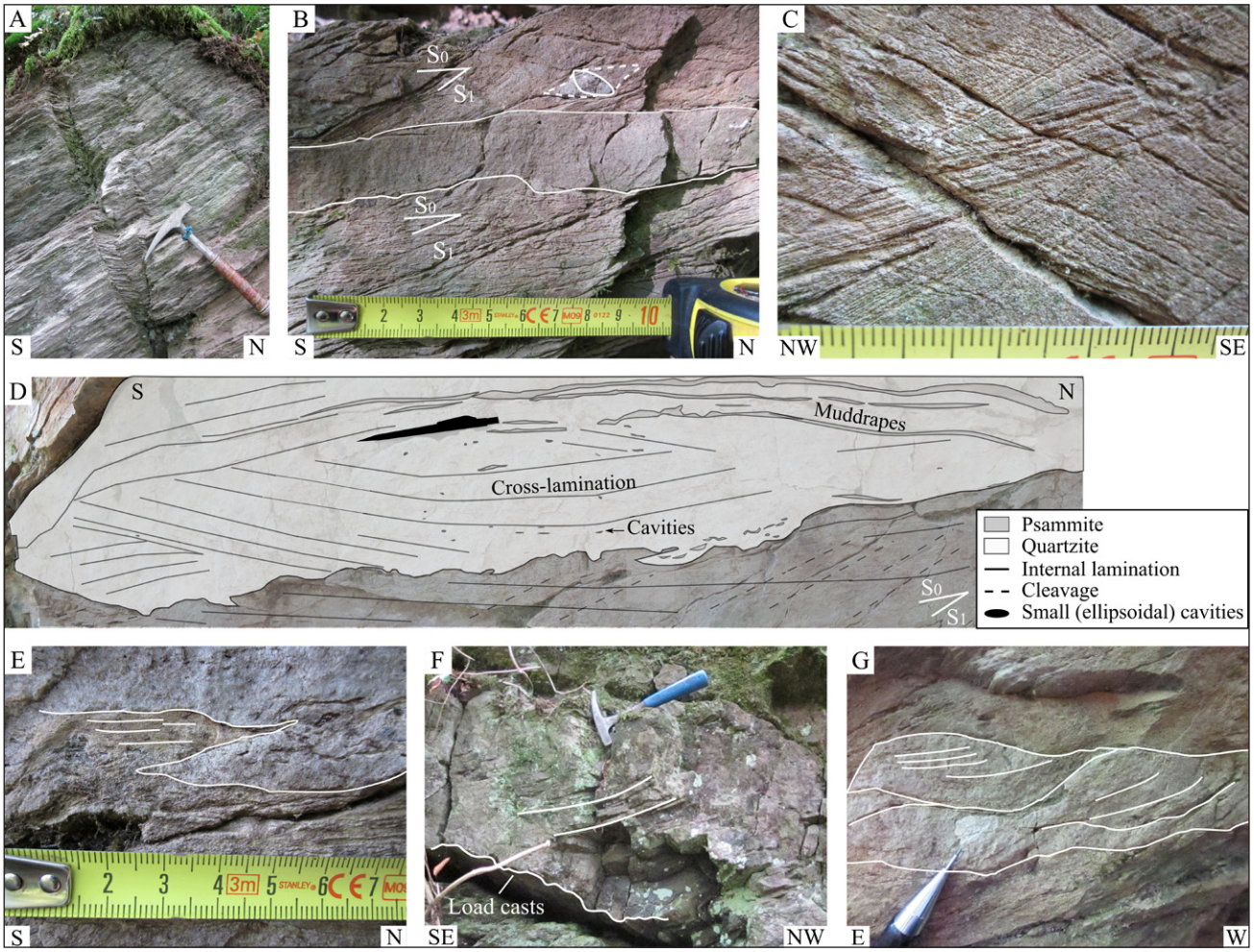

Figure 3. Lithology and sedimentary structures. (A) Metapelites with a penetrative, south-dipping, slaty cleavage, containing kink bands. (B) A 2 cm thick, quartzitic layer (full lines) embedded in a psammite sequence. A sandball and its pressure shadows are outlined (dashed lines). (C) Internal planar- and cross-lamination in psammite, indicating a normal stratigraphic polarity. (D) A cross-bedded quartzitic layer showing three generations of oppositely dipping cross-beds. Mud-drapes are parallel to the cross-beds. Soft-sediment deformation structures (e.g. flame structures and disturbed bedding) are present at the lower contact of the quartzitic sandstone with the psammite. (E) Flame structure pictured in (D). (F) Quartzitic layer showing internal cross-bedding and load casts. (G) Quartz-rich gullies with tangential cross-lamination, indicating a normal stratigraphic polarity. Tape measure, hammer (29 cm) and pencil (15 cm) for scale.

soft-sediment deformation structures (e.g. flame structures and disturbed bedding) can be observed (Fig. 3D-E). The quartzitic sandstones show no systematic ordering, and their bedding can be defined as lenticular (isolated to connected) in a dominant silt-rich matrix (cf. Reading, 1996).

4. Structural analysis

4.1. Fold train

The first-order fold train along the 2.5 km long section (Fig. 2A) has been reconstructed by mapping the geometry of higher-order, parasitic folds. The fold train consists of strongly asymmetric folds with weakly dipping backlimbs and steeply dipping, short forelimbs (Fig. 2B). These first-order, north-verging step folds are relatively open, with moderately south-dipping, axial planes and sub-horizontal hinge lines with a variable plunge. A non-axial planar cleavage, transecting the fold hinges obliquely, has been observed locally. Three fold zones are well exposed (Fig. 2): (1) a monocline (see paragraph 4.2), (2) folds associated with a lenticular, competent body (see paragraph 4.3) and (3) an overturned syncline (see paragraph 4.5).

The fold train observed can be fitted within the regional structural context of the 'Redu Syncline' proposed by Asselberghs (1946), in which it occupies the central part. In style, the 'Redu syncline' is considered a transitional structure between the Dinant fold-and-thrust belt in the north and the backbone of the Ardenne culmination in the south (Fig. 4). It is bounded by the inferred Opont fault to the south and the inferred Vencimont fault to the north, both interpreted by Beugnies (1985) as major south-dipping reverse faults in the Ardenne culmination.

Structural mapping reveals that the fold train in this northwestern part of the Ardenne culmination is non-cylindrical in nature (Fig. 5). This is expressed by (1) a periclinal first-

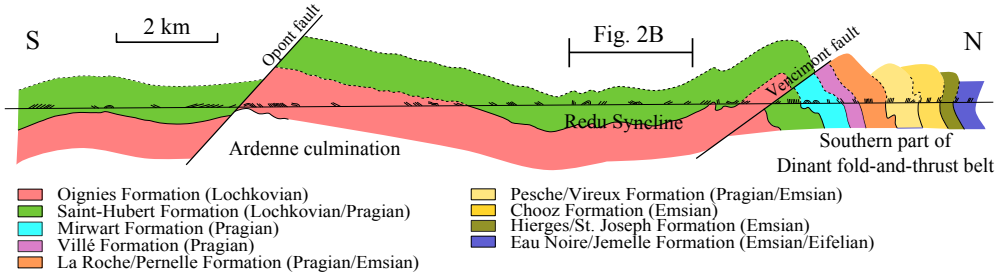

Figure 4. The position of the 'Redu syncline' as defined by Asselberghs (1946), in the structural transition from the Ardenne culmination in the south to the southern part of the Dinant fold-and-thrust belt in the north (adapted after Asselberghs, 1946). The position of the structural section studied (Fig. 2B) is marked.

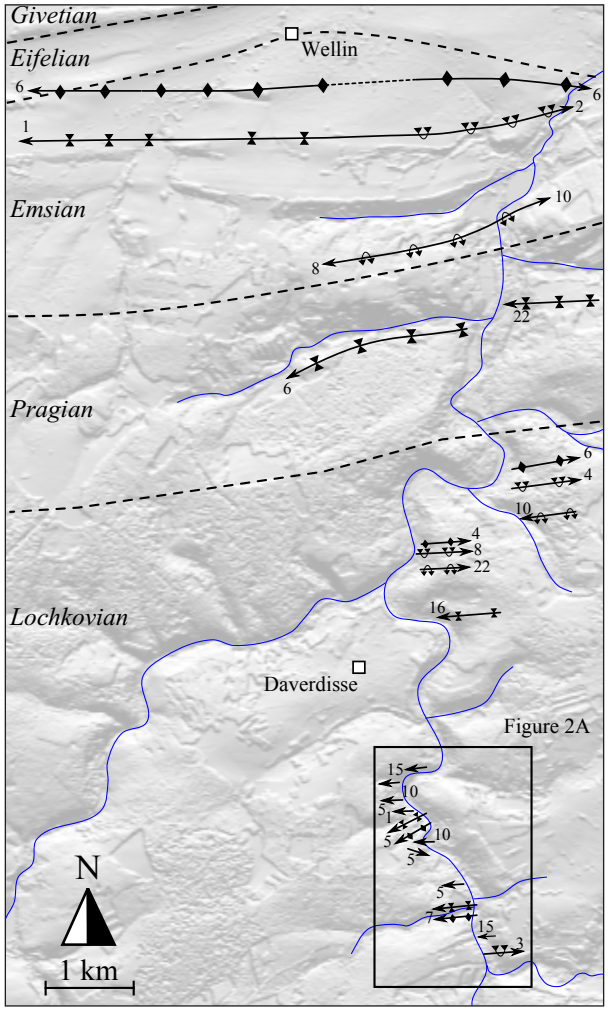

Figure 5. Fold geometry in the northern part of the Ardenne culmination (to the north of the study area - cf. box), indicating the occurrence of double-plunging, en-echelon folds with varying fold hinge plunges. Orientation of fold hinges and bedding-cleavage intersection lineations are added. The borders of the stratigraphic units, according to our own observations, have been marked (dashed lines).

order fold geometry in an en-echelon configuration, (2) variable fold hinge plunges with adjacent fold pairs commonly plunging in opposite directions, and (3) a variable degree of folding. En-echelon folds are a special case of doubly plunging, non-cylindrical folds, typified by hinge lines that laterally change curvature. As such, folds may disappear or change from an antiform to a synform laterally along the trend of plunge. When additional folds are developed, these changes in plunge result in en-echelon folds, with a gradually opening fold being replaced by a neighbouring, gradually tightening fold of opposite form (van der Pluijm & Marshak, 1997). The latter is exemplified just south of Wellin, where a first-order syncline is strongly overturned to the east of Wellin but gradually changes to an open syncline with normal structural polarity to the west of Wellin (Fig. 5). Further evidence of non-cylindrical folding becomes apparent on a more local scale in the different exposures.

4.2. Exposure A

Observations and measurements

The folding kinematics active during the Variscan orogeny are well illustrated in a series of three outcrops (Fig. 6A), showing, on the one hand, a slightly buckled 2 metre-thick quartzitic layer (Fig. 6B), and, on the other hand, highly folded multilayer sequences,

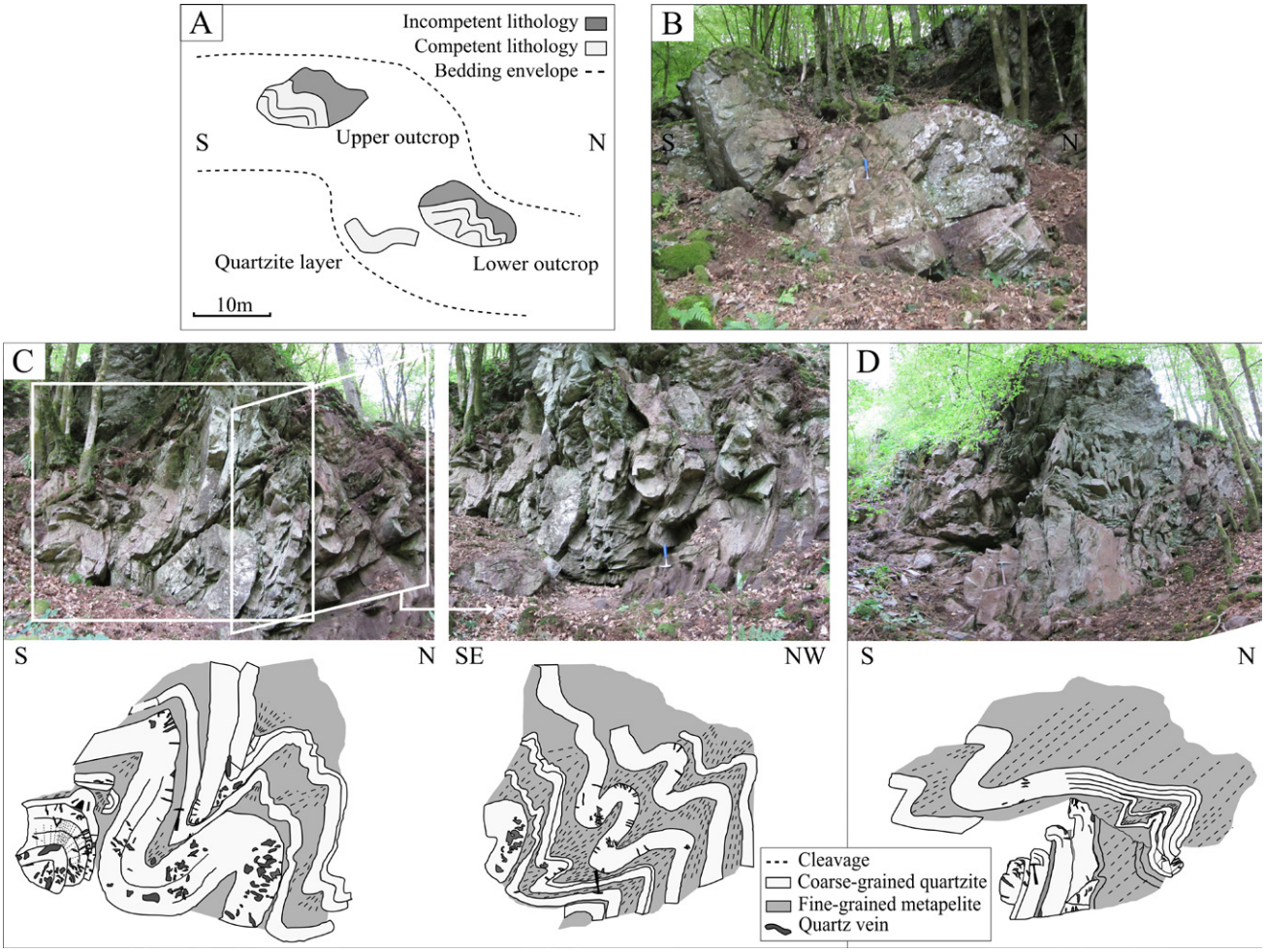

Figure 6. Exposure A - Overview photographs and line-drawings of the monocline. See Fig. 2 for location. (A) Line-drawing of the different outcrops and their large-scale structural interpretation (dashed lines). (B) Photograph of the thick folded quartzitic bed to the south of the lower outcrop. (C) Overview photographs and line-drawings of the S-N (left) and SE-NW (right) sections of the lower outcrop, and (D) of the S-N section of the upper outcrop. Hammer (29 cm) for scale.

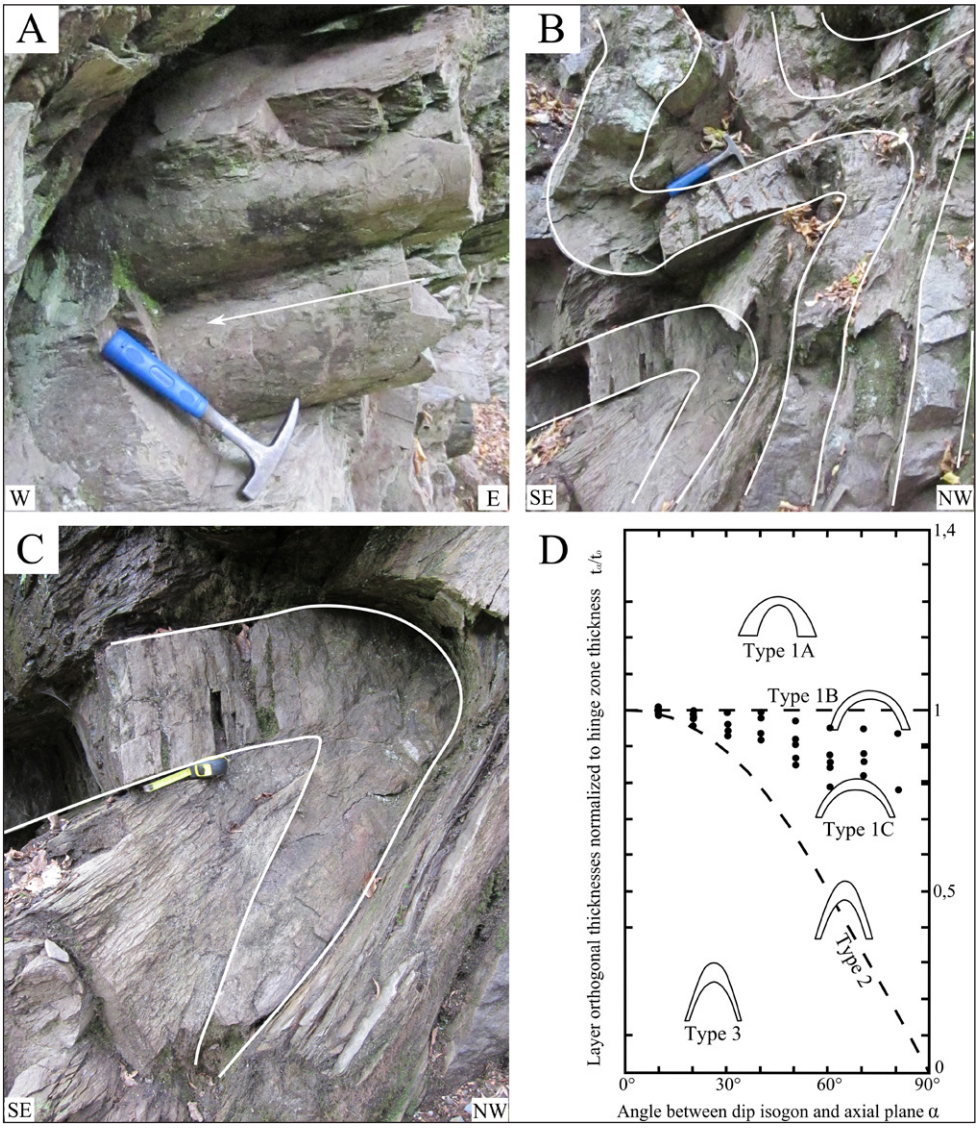

Figure 7. Exposure A - Structures and measurements specifying folding kinematics. (A) Fold boudins, developed by the high-frequency folding of quartzitic sandstones. The cusps, marked with a white arrow, dip to the west. (B) Alternation of competent and incompetent layers, maintaining their thickness (class 1B) and being thickened in the hinge zones (class 2), respectively. (C) A folded quartzitic layer wedging out to the north. Hammer (29 cm) and tape measure for scale. (D) Dip-isogon analysis of folded competent beds demonstrating the presence of 1C type folds (after Ramsay, 1967).

exposing M-type (lower outcrop; Fig. 6C) and Z-type, north-verging (upper outcrop; Fig. 6D), second-order parasitic folds. These parasitic folds are a patchy reflection of a monocline within the fold train (Fig. 6A). The multilayer sequence is strongly influenced by polyharmonic folding, with a variable layer thickness giving rise to folds of different amplitudes but with more or less continuous axial surfaces. The lower outcrop shows the strongest degree of polyharmonic folding, especially on top of the thickest quartzitic layer (Fig. 6C) where thinner layers form high-frequency 'fold boudins' (Fig. 7A). In contrast, the 2 metre-thick quartzitic layer has a much larger fold amplitude (Fig. 6A-B). The incompetent lithology in these outcrops shows a very well-developed slaty cleavage, with a consistent divergent fanning pattern in the fold hinge zones (Fig. 7B). The competent quartzites in general do not show any mesoscopic cleavage, except in one case where a convergent fanning fracture cleavage was observed in the inner arc of a thick, folded quartzitic layer (Fig. 8A).

Throughout both the upper and lower outcrops the incompetent material is preferentially thickened in the hinge zones (i.e. class 2 fold type - e.g. Ramsay, 1967) (Fig. 7B). The quartzitic layers, however, approximately maintain their original thickness. The latter is confirmed by a dip isogon analysis on the quartzitic layers, which demonstrates that in general we are dealing with a transition from 1B to 1C type folds (Fig. 7D). In two cases constant thickness is not preserved. On the one hand, some anomalously thin competent layers show a pinch-and-swell morphology parallel to bedding (Fig. 8A), indicating layer-parallel boudinage. In the thinned parts of these layers bedding-perpendicular veins occur. On the other hand, a specific lenticular quartzitic layer wedging out to the north was encountered in the lower outcrop (Fig. 7C).

A broad range of different fold-related quartz vein types were identified within exposure A, and have already been extensively discussed by Jacques et al. (2014). These veins are consistently limited to the competent rocks or their interface. At the interface of the quartzitic layers, firstly, we observed (1) slickenfibres with a reversed slip sense on opposite fold limbs, and (2) saddle reef veins between adjacent quartzitic layers of contrasting thickness (Fig. 8A-B). Within the quartzitic layers, secondly, we observed (1) extensional extrados veins in the outer arcs of fold hinges (Fig. 8B), (2) the already mentioned bedding-perpendicular veins within the boudinaged quartzitic layers (Fig. 8A), and (3) a complex array of extension veins associated with a bedding-parallel hinge thrust (Fig. 8C).

Bedding measurements describe a girdle distribution with a calculated β-fold axis of 264/07 (Fig. 9A). The measured fold hinge lines, however, with an average value of 264/08, show a considerable departure in orientation from the calculated fold axis. Cleavage measurements have an average value of 177/45, approximately axial planar to the bedding girdle (Fig. 9A). Slickenfibre lineation measurements, present on most of the fold limbs, show a well-defined girdle distribution of 070/66, and an accompanying calculated slickenfibre π-axis (e.g. Tanner, 1989) of 250/24 (Fig. 9B).

Interpretation

The structural features observed are indicative for different folding mechanisms. Firstly, tangential longitudinal strain (i.e. contraction and extension in the outer and inner arc of a buckled layer, respectively – cf. Hudleston & Treagus, 2010) of the competent quartzitic layers has been identified by (1) the extrados veins originating from outer arc stretching (Fig. 8B), and (2) the intensification of a fracture cleavage on the inner arc of a fold

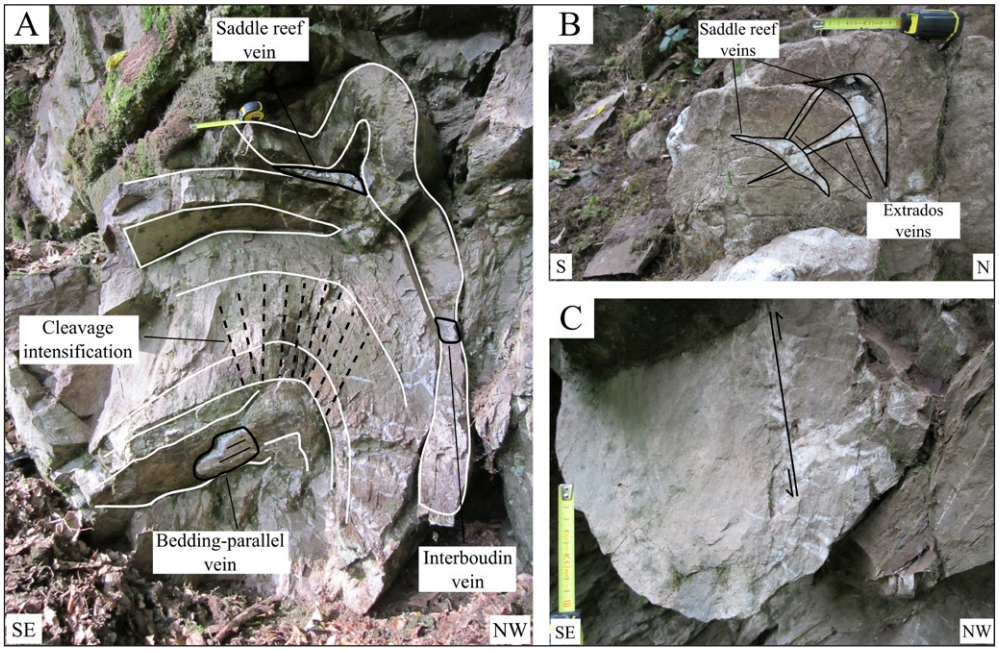

Figure 8. Exposure A - Fold-related structures and veins, observed in the outcrops of the monocline. (A) Quartzitic beds (bedding is marked in white) showing different quartz vein types, a dilated hinge zone, boudins and fracture cleavage intensification. (B) Fold hinge zone with associated saddle reef veins and extrados veins. (C) Chaotic veining, associated with a synclinal hinge thrust. Hammer (29 cm) and tape measure for scale.

hinge (Fig. 8A) (e.g. Ramsay, 1974). Secondly, flexural flow is evidenced by the preferential thickening of the incompetent material in fold hinge zones (Fig. 7B) (e.g. Ramsay, 1967). Thirdly, flexural slip is demonstrated by (1) the presence and slip sense of the slickenfibres (e.g. Tanner, 1989), (2) hinge dilation between adjacent quartzitic layers of contrasting thickness with saddle reef veining as a result (Fig. 8A-B), (3) boudinage of anomalously thin quartzitic layers with associated bedding-perpendicular veining in the interboudin necks (Fig. 8A), and (4) the complex array of extension veins associated with a hinge thrust (Fig. 8C). The latter features serve to accommodate the spatial problem during flexural-slip folding of layers with variable layer thickness and small interlimb angles (Ramsay, 1974).

Contrary to what would be expected in the case of flexural-slip folding with bedding-parallel slip orthogonal to the hinge line (Tanner, 1989), the π-axis orientation is different from the orientation of the calculated β-fold axis with an angular offset of 22° (Fig. 9B). Despite this angular difference, the slickenfibre lineation can still be linked to the flexural-slip mechanism because (1) the slickenfibres are consistently observed on both fold limbs but cannot be retrieved in the fold hinge zones, where the amount of slip should equal zero during flexural slip (Fowler, 1996; Tanner, 1989), and (2) the slickenfibre step sense is consistently reverse on opposing fold limbs. Therefore the slickenfibre lineations are indicative of oblique flexural slip.

Such an oblique slip sense can be explained by three mechanisms. Ramsay (1967), on the one hand, explained oblique flexural slip by previously inclined beds or an irregularity in layer thickness. A second option would be that the fold structures and slickenfibre sheets are a reflection of superimposed kinematic events. The slickenfibres could have developed early in the folding history, with later rotation of the shortening axis, or the slickenfibre sheets could show horizons of variable slickenfibre lineations, representing different phases of folding. Thirdly, the geometry of non-cylindrical folds can also give rise to a variable slickenfibre orientation according to their position on the fold structure and their timing. The slip direction in the latter case will only be perpendicular to the fold hinge within fold culminations and depressions (Tanner, 1989) (Fig. 9C). Considering these three options, the second option of superimposed kinematic events can already be dismissed based on the observations that (1) the slickenfibre lineation does not vary in orientation in a cross-cut along different quartz vein sheets (cf. Jacques et al., 2014), and (2) because flexural slip occurred only in the latest stage of folding (upon lock-up) (cf. microthermometric data on saddle reef veins – Jacques et al., 2014); hence the slickenfibres cannot represent an early stage in the folding history with later rotation of the shortening axis. For both the first and last option, indications can be retrieved in the field. Within the folded sequence a

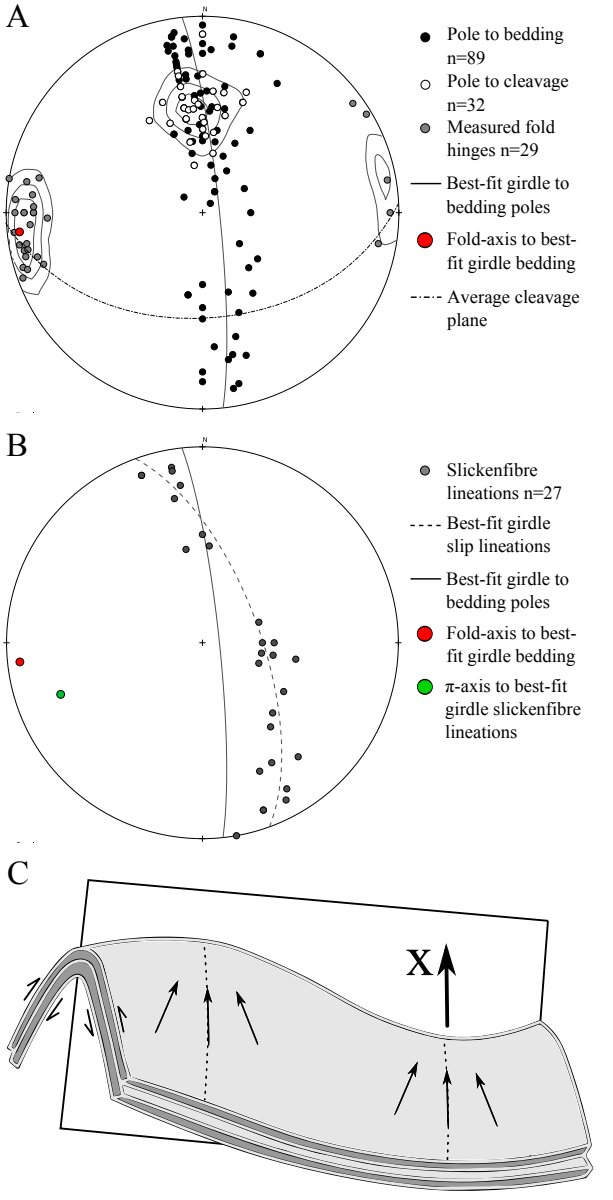

Figure 9. Exposure A. (A) Lower-hemisphere equal-area stereographic projection of orientation data of bedding and cleavage. (B) Lower-hemisphere equal-area stereographic projection of the slickenfibre lineations. (C) The geometry of oblique flexural slip in non-cylindrical folds. Adapted after Tanner (1989).

wedging quartzitic layer has indeed been observed (Fig. 7C). The variable inclination and limited continuity of such a lenticular competent layer, not uncommon in the study area (see paragraph 3), could lead to oblique slip relative to the overall fold hinge. However, indications of double-plunging, curvilinear folds were also observed, as expressed by the variability of the measured fold hinge lines (Fig. 9A). Hence, both options seem plausible, although it should be expected that the variable inclination of lenticular layers would have resulted in more irregular slickenfibre girdle distributions than observed (Fig. 9B). Because regionally also other evidence for non-cylindrical folding is observed (cf. paragraph 4.1), we lean towards the last option.

Finally, the dip-isogon analysis shows that we are dealing with a transition from 1B to 1C type folds for the competent quartzite layers (Fig. 7D), indicative of the migration of material from the fold limbs to hinges. This migration could either be related to volume-loss folding because of the competence contrasts with the incompetent layers (e.g. Twiss & Moores, 1992) or a superimposed homogeneous flattening (or passive amplification) to accommodate further flexure after fold lock-up (e.g. Ramsay, 1967).

4.3. Exposure B

Observations and measurements

The second exposure consists of an alternation of quartzitic sandstones, psammites and slates (Fig. 10). The psammite shows a planar and cross-lamination - indicating a normal stratigraphic polarity - and a spaced cleavage. Three distinct layers of quartzitic sandstones were observed. The first, lowermost quartzitic layer (**1**) is only weakly deformed and has preserved its sedimentary structures (i.e. cross-bedding and load casts – Fig. 3F). A second quartzitic layer (**2**) is strongly faulted with an internal bedding, which is only locally observable (Figs 10 & 11A). Finally, a third quartzitic layer (**3**) has a lenticular shape, wedging out abruptly to the north within the psammites (Figs 10 & 11A). To the south, however, the layer lies in direct contact with the underlying, faulted quartzitic layer (**2**) (Fig. 11A). Internal bedding in this wedge is present at a high angle in the toe of the wedge, while being parallel away from the toe (Fig. 11).

On an outcrop-scale, a first-order gentle and open fold geometry is observed (Figs 2B & 10), best reflected by the north-verging, Z-shape of the lenticular body (**3**). This fold has

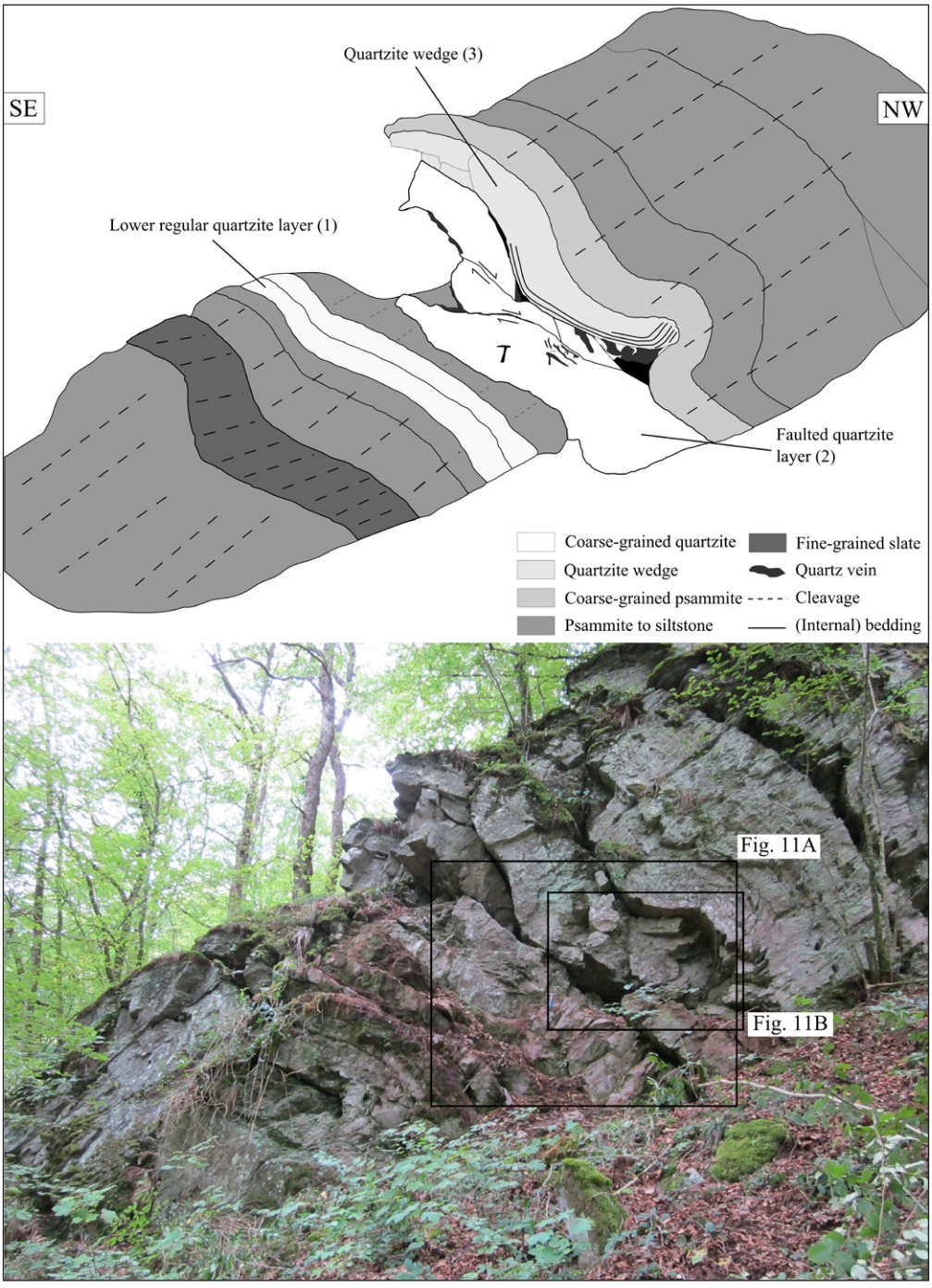

Figure 10. Exposure B - Overview line-drawing and photograph. See Fig. 2 for the location.

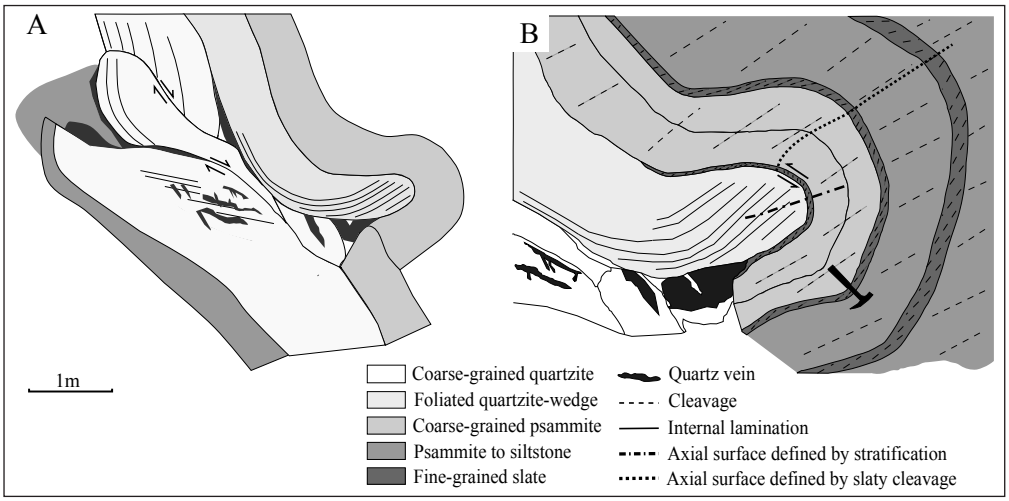

Figure 11. Exposure B - Detailed line-drawings of structures. (A) The centre of the outcrop, with specific attention to the faulted quartzitic layer and its internal bedding. (B) The toe of the wedge and the surrounding secondary fold in the incompetent lithology. The discrepancy between the axial planar slaty cleavage (cf. thin slate layers) and the axial plane defined by stratification is indicated. Hammer (29 cm) for scale.

a consistently north-dipping bedding that describes a girdle distribution (060/85) with a west-plunging β-fold axis (240/05) (Fig. 12A). The associated cleavage, with an average of 191/37, is clearly non-axial planar. The cleavage transection is illustrated best by the difference between the measured orientations of the bedding-cleavage intersection lineation (average value of 273/06) and the calculated β-fold axis orientation (Fig. 12A) (e.g. Johnson & Woodcock, 1991). The average offset angle between both equals 33°. Within the more incompetent rocks surrounding the toe of the quartzitic wedge to the north, a small-scale, second-order fold is superposed on the outcrop-scale first-order fold (Fig. 11B). This second-order fold has a bedding girdle, with a calculated β-fold axis of 063/82 (Fig. 12B), similar to that of the regional first-order fold. Within the thin pelitic layers a divergent slaty cleavage fan is apparent (Fig. 11B). The average orientation of the secondary cleavage is 166/46 (Fig. 12B), which is axial planar to the second-order fold, as indicated by the correspondence of the orientation of the bedding-cleavage intersection lineation and the calculated β-fold axis orientation (Fig. 12B). The secondary slaty cleavage, however, does not directly coincide with the axial plane of the second-order fold formed along the toe of the wedge (Fig. 11B).

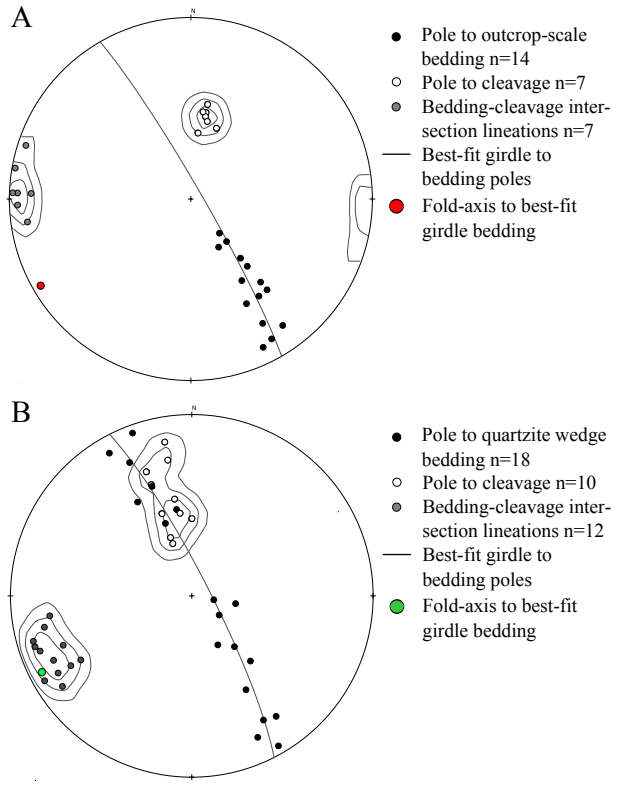

Figure 12. Exposure B - Lower-hemisphere equal-area stereographic projections of orientation data of the first-order, outcrop-scale fold (A), and of the second-order fold at the toe of the wedge (B).

Interpretation

The three quartzitic layers show a different morphology of internal bedding, which can be the result of a specific degree or style of deformation. Layer (**1**) shows a planar cross-bedding and is only slightly folded (Figs 3F & 10). The lenticular layer (**3**), showing an internal bedding that changes from parallel along its central part to a high angle at its toe, could be considered as an initially lenticular body with tangential cross-bedding, similar to layer (**1**) (step 1; Fig. 13A). Top-to-the-north shearing during contraction folded this original lenticular body into a wedge with a Z-shaped geometry. During folding, cross-bedding is passively rotated, becoming parallel to bedding in the central part of the wedge. Because of the limited rotation of the toe of the wedge, cross-bedding maintained its initial high angle to bedding (step 2; Fig. 13A). This type of passive-marker deformation of oblique foliations (e.g. cross-bedding) has earlier been studied and described in detail (Aller et al., 2010; Bobillo-Ares et al., 2009; Ramsay, 1961; Williams, 1979).

In a similar manner, the kinematic evolution of the faulted layer (**2**) is considered (Fig. 13B). Again assuming an original quartzitic layer with cross-bedding (step 1), top-to-the-north shearing caused tilting and slight folding of the initial layer with minor passive rotation of cross-bedding, in an opposite way within both bends (step 2 & 3; Fig. 13B). At some point during folding, the high competence of the quartzitic sandstone caused brittle failure. A certain degree of folding must had occurred already, since the observed faulted segments have a considerable degree of curvature (Figs 10 & 11A). Brittle failure occurred at both interfaces in the vicinity of the fold hinges where strain is concentrated during folding (step 4 & 5; Fig. 13B).

Taking into account the kinematics of both quartzitic layers, the evolution of the entire succession can be reconstructed (Fig. 13C). The initial sedimentary succession consisted of (sub) horizontal layers of coarse quartzitic sandstones, of which one has a lenticular shape, embedded in a more incompetent psammitic matrix (step 1; Fig. 13C). As contraction started, simple shear was transmitted on the horizontal layers (step 2; Fig. 13C). The presence of a lenticular body, acted as the nucleation point of folding (step 3; Fig. 13C). Because the lenticular body was easier folded due to its lateral extremities, it detached from the underlying layer with the contact becoming a slip surface (step 4; Fig. 13C). Hence, the incompetent material passively folded around the toe of the wedge in front of the propagating lenticular body and the observed second-order slaty cleavage developed (step 5; Fig. 13C). Because of this direct kinematic link with the lenticular body, the second-order cleavage is axial planar to the bedding girdle, in contrast to the first-order non-axial planar, transecting cleavage. By building shear stress, layer (**2**) eventually also underwent internal brittle failure, resulting in the displacement of three faulted segments (step 6; Fig. 13C). The orientation difference between the second-order, slaty cleavage and the axial plane defined by the stratification of the wedge

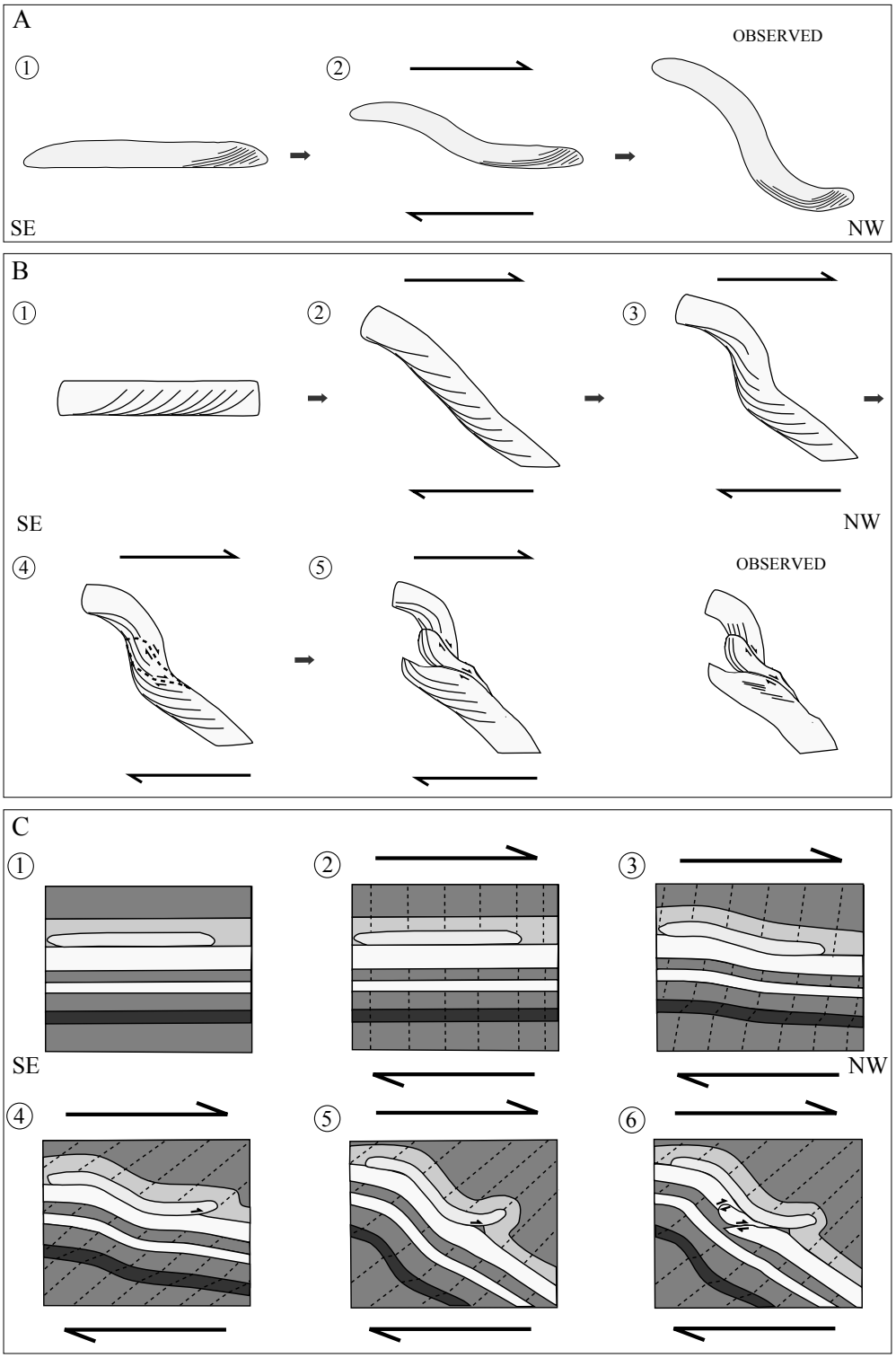

Figure 13. Exposure B - Evolutionary sketches of the kinematics. (A) Due to top-to-the-north simple shearing, the lenticular layer (**3**) is progressively rotated in a clockwise sense with internal cross-bedding undergoing passive rotation. (B) Folding of the quartzitic layer (**2**) is accommodated by brittle failure along two interfaces after a certain amount of buckling. The observed internal bedding geometry originates from passive rotation of the initial cross-bedding, with subsequent displacement by faulting. (C) Evolutionary model compiling the kinematics for the total outcrop geometry. See text for further explanation.

(Fig. 11B), is probably related to an additional penetration of the wedge after the formation of the second-order cleavage. Taking into account the displacement sense of the wedge relative to the second-order cleavage (Fig. 11B), the angular difference is most likely linked to the faulting and the imbrications of the resulting fault wedges.

4.4. Exposure C

Observations and measurements

A third exposure consists of the superposition of a coarse-grained psammite, a thin intermediate layer of fine-grained shale and a coarse-grained quartzitic sandstone (Fig. 14A-B). The thickness of the quartzitic beds is variable, thinning out downdip (to the north). No cross-bedding is discernible within the quartzitic beds. Cross-lamination, however, is present in the psammite lithology, and indicates a normal stratigraphic polarity.

In the central part of the outcrop, an irregular quartzitic wedge lies in direct contact with the overlying psammite and metapelite and is disconnected from the underlying quartzitic sandstone layer (Fig. 14A-B). Downdip, a large lenticular quartz vein, composed of blocky crystals with well-developed crystal faces, is present at the toe of the wedge (Fig. 14C) (Jacques et al., 2014). Updip, the transition to the quartzitic sandstone is rather diffuse with brecciation of the quartzitic sandstone and associated irregular veining (Fig. 14C). At the contact of the tectonic wedge with the underlying quartzitic beds, slickenfibres are visible (Fig. 14D). In front of the quartzitic wedge, a gently buckled small-scale fold is developed within the metapelite and psammite (Fig. 14A-B). In the hinge zone of this small-scale fold, the cleavage shows divergent fanning. An angular difference of the average cleavage orientation (191/33) with the best-fit girdle to the bedding poles suggests that cleavage is weakly transecting, with an offset angle of 10° relative to the bedding girdle (Fig. 15). This is confirmed

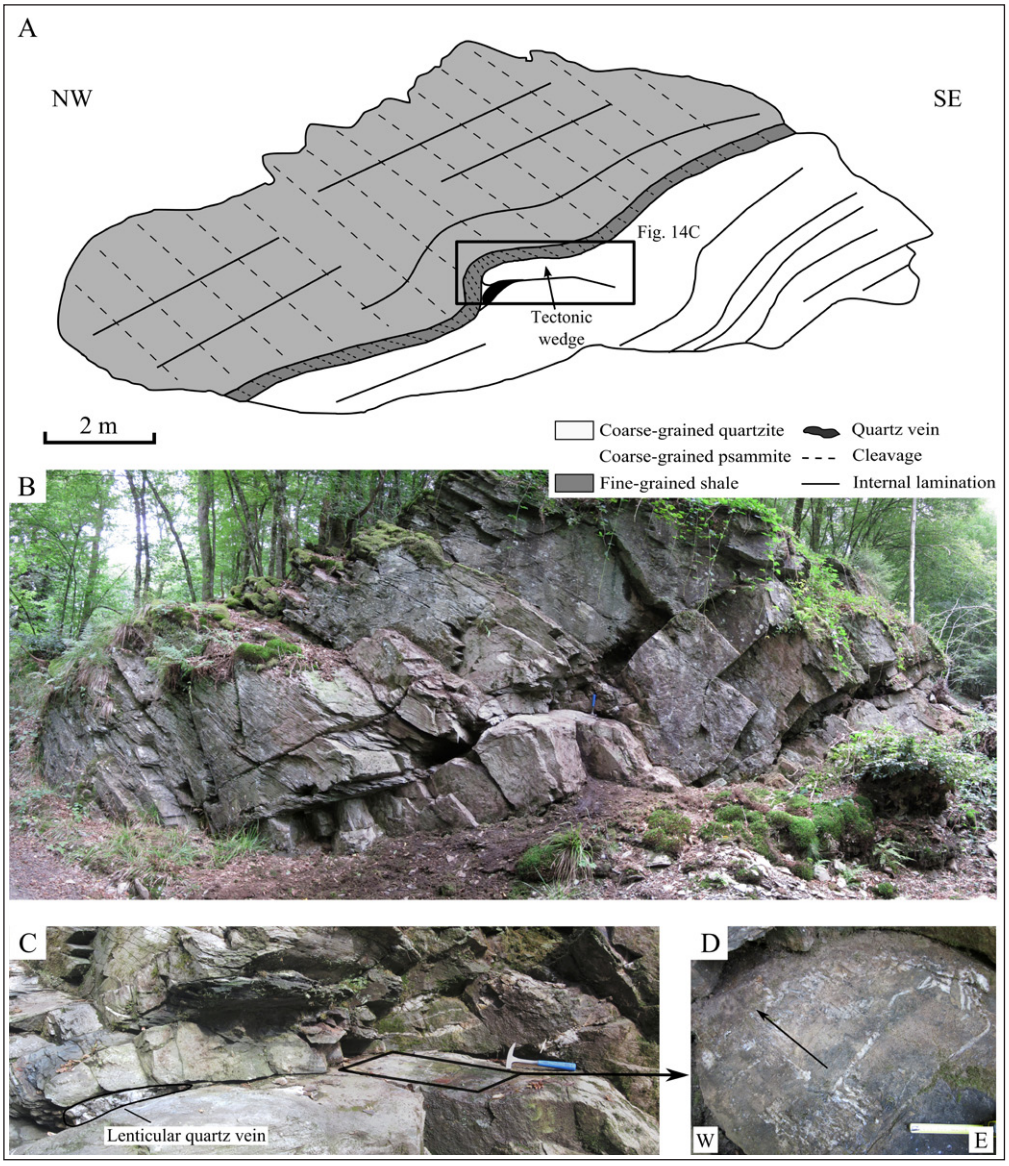

Figure 14. Exposure C - Structures and veins associated with the tectonic wedge. See Fig. 2 for the location. (A,B) Overview line-drawing and photograph of the outcrop. (C) Tectonic wedge with the accompanying down- and updip presence of a lenticular quartz vein and internal brecciation with associated chaotic veining, respectively. (D) Slickenfibres on the fault contact of the lower quartzite beds with the tectonic wedge, indicating reverse top-to-the-north slip towards the small-scale fold. Hammer (29 cm) for scale.

by the bedding-cleavage intersection lineations, with an average intersection lineation (266/09) that is clearly offset relative to the calculated fold axis (256/07) of the well-defined bedding girdle (Fig. 15). The quality of the data is confirmed by the accordance of the average cleavage plane (191/33) with the average bedding-cleavage intersection lineation (Fig. 15).

Fault plane- and slickenfibre orientations are very consistent, having average values of 241/19 and 167/08, respectively (Fig. 15). When comparing these data with the bedding girdle of the small-scale fold (with a calculated β-fold axis of 256/07), it can be concluded that (1) the slickenfibre orientation is subparallel with the strike of the girdle (i.e. perpendicular to the strike of bedding) and (2) that the fault planes and the bedding girdle have approximately the same strike (Fig. 15).

Interpretation

The presence of the slickenfibres at the bottom of the quartzite wedge and the irregularity of the bedding-truncating wedge, indicate that the contact of the wedge with the underlying quartzitic sandstone is a fault plane. The position of the small-scale fold and its divergent cleavage fan in front of the tectonic wedge, moreover, indicate an obvious kinematic relation between the small-scale fold and the tectonic wedge. The orientation analysis indicates that the bedding-truncating fault plane and the small-scale fold both propagated subparallel to the dip direction of bedding.

We interpret bedding-parallel shear during folding as the driving force behind initiation of the tectonic wedge (Fig. 16). As the outcrop is present in the northern normal limb of a first-order overturned syncline (Fig. 2A-B), the consistent top-to-the-north shear, observed on the fault plane (Fig. 14D), corroborates out-of-syncline shearing, resulting in the tectonic wedge. The initiation of the tectonic wedge is most probably related to the highly competent behaviour and consistent thickness variations (thinning out downdip to the north) of the quartzites, most likely corresponding to a metre-scale point bar succession. Parasitic folding of these point bars would have led to accommodation problems and top-to-the-north bedding-parallel shear, leading to bedding-parallel brittle failure and the formation of the tectonic wedge (Fig. 16). The emplacement of the lenticular quartz vein

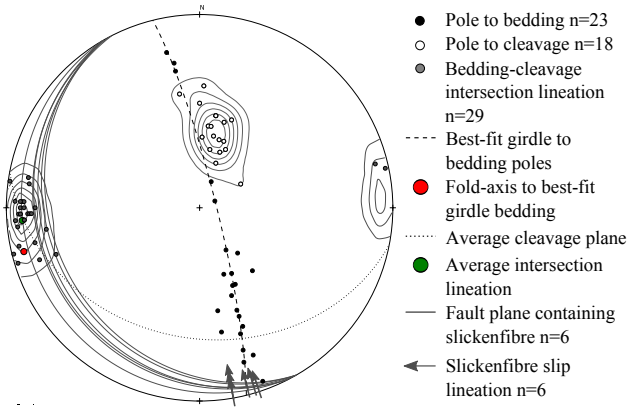

Figure 15. Exposure C - Lower-hemisphere equal-area stereographic projection of orientation data, showing the geometric relationship between the faulted wedge and the small-scale fold.

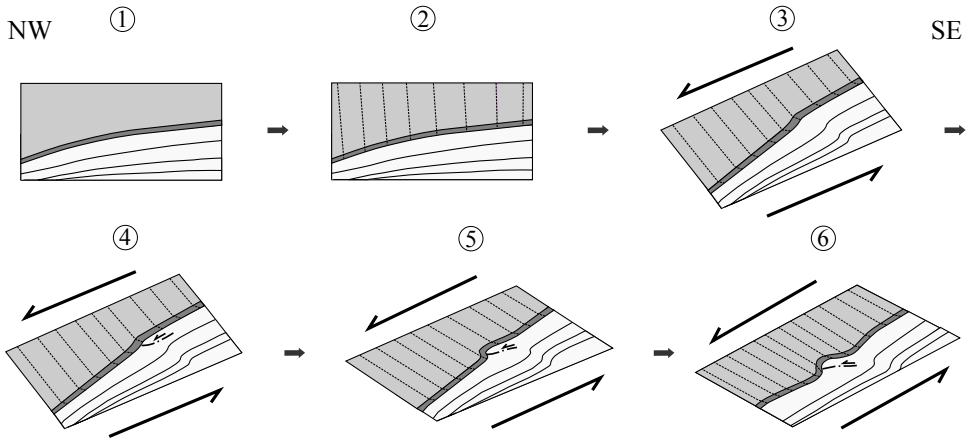

Figure 16. Exposure C - The proposed kinematic model for the (parasitic) folding of the point bar succession (step 1-3), the formation of a tectonic wedge (step 4), and associated small-scale folding and quartz veining (step 5-6).

indicates that the thrust fault did not continue into the metapelite, which is corroborated by the continuity of the metapelite layer around the wedge (Fig. 14A). As confirmed by the orientation analysis and their obvious geometric relation, nucleation of the small-scale fold is related to passive folding of the incompetent metapelite and psammite along the propagating tectonic wedge (Fig. 16).

4.5. Exposure D

Observations and measurements

A fourth exposure, illustrating a disharmonically folded multilayer sequence, consists of three zones (Fig. 17A-D): (1) a transition from a regular cross-bedded quartzitic layer, to a thick quartzitic layer that is folded into a nearly isoclinal, second-order fold, as marked by the irregular internal bedding; (2) a thick layer of less folded psammite with a clearly developed spaced cleavage (Fig. 18A); and (3) several regular quartzitic layers, asymmetrically folded into a strong Z-shaped, north-verging geometry. The asymmetry of these parasitic folds, i.e. the Z-shape of the weakly folded psammite layer, and the inverse stratigraphic polarity of the cross-bedded quartzitic layers (Fig. 18B) confirm that the outcrop is part of the southern steep limb of a first-order overturned syncline (Fig. 2A-B).

Orientation data support this structural interpretation (Fig. 17E). Bedding measurements describe a girdle of 267/88, and a corresponding east-plunging β-fold axis of 087/02. Bedding-cleavage intersection lineation orientations are variable east- to west-plunging, with an east-plunging average value of 082/00 (Fig. 17E). An overall eastern plunge of the first-order overturned syncline complies with the observed parasitic Z-fold asymmetry. Cleavage orientations have an average value of 188/41. Based on the offset between the average bedding-cleavage intersection lineation and the calculated fold axis, an angular difference of 5° between the cleavage and the bedding girdle is calculated, which suggests that the cleavage is weakly transecting (Fig. 17E). However, due to the bad fit of the bedding measurements to the girdle (a weak strength parameter of 3.68 according to the Woodcock eigenvalue classification - Woodcock, 1977) and the fact that the average cleavage plane does not contain the average

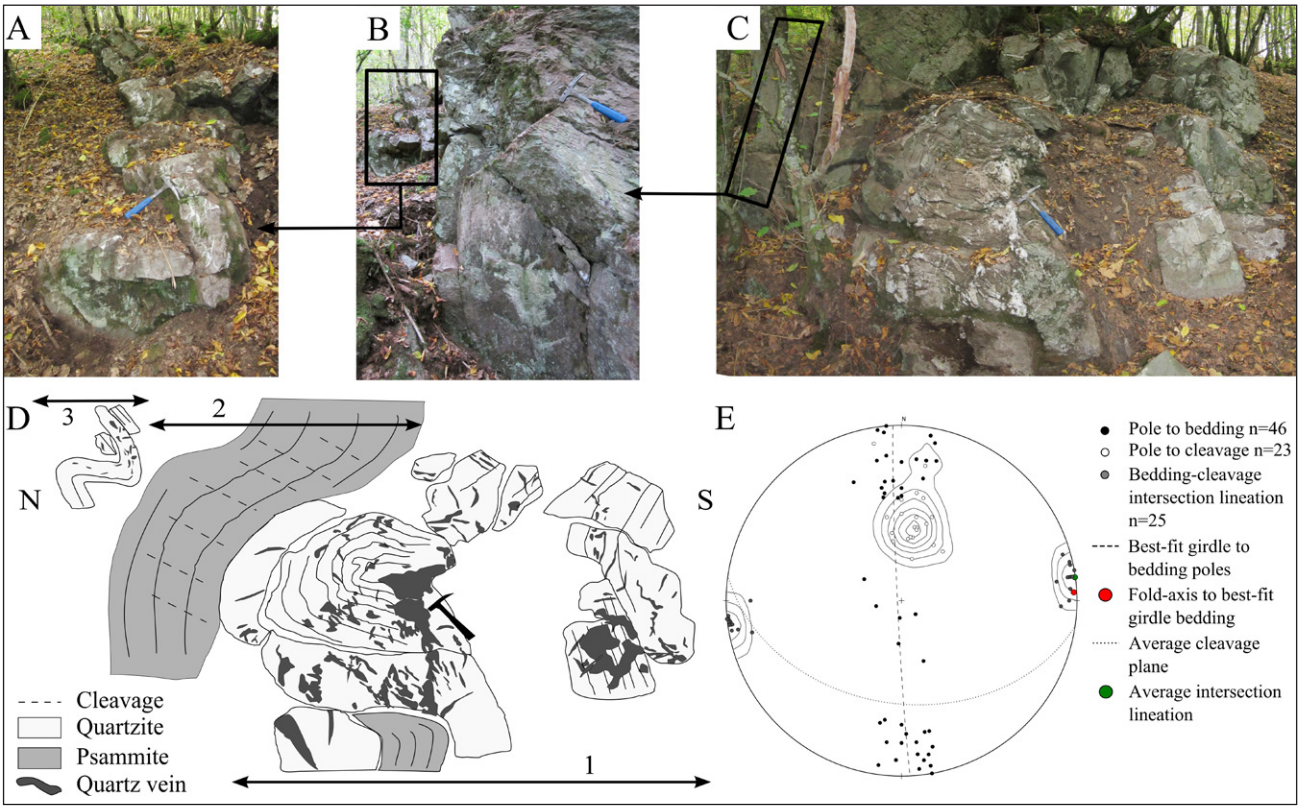

Figure 17. Exposure D - Structure and orientation data. See Fig. 2 for the location. (A-D) Overview photographs and line-drawing of the outcrop containing abundant stockwork veining. Because of limited visibility, the outcrop is divided over three photographs (A to C) from north to south. (D) Schematic line-drawing of the total structure, with indication of zones 1 to 3. Hammer (29 cm) for scale. (E) Lower-hemisphere equal-area stereographic projection of related orientation data.

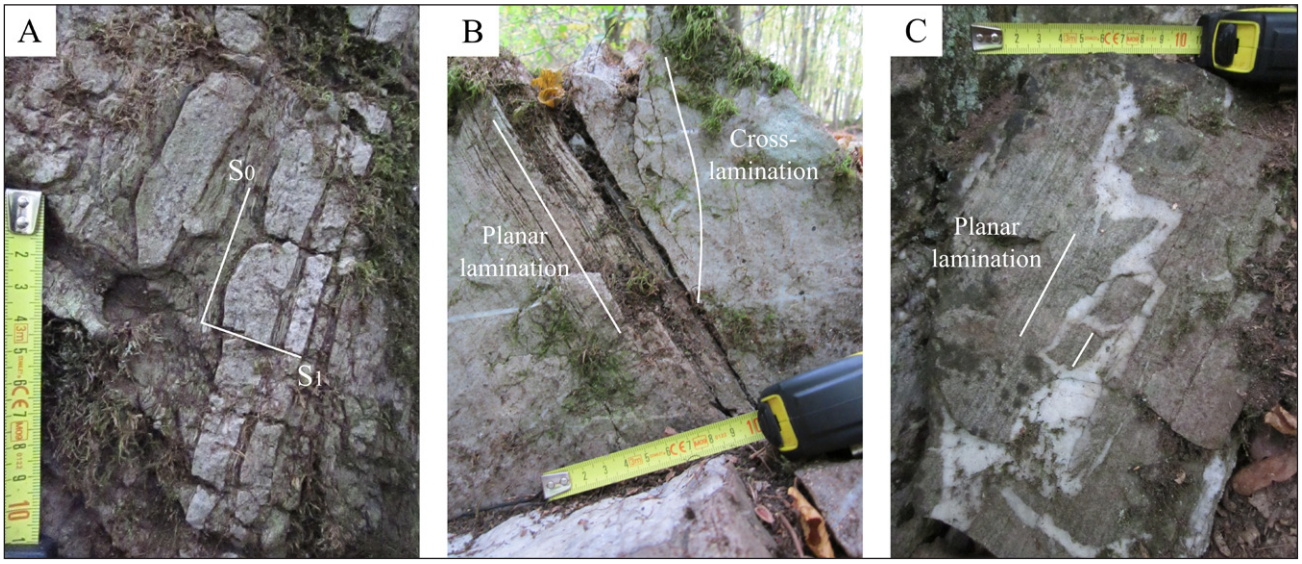

Figure 18. Exposure D - Sedimentary structures and stockwork veining. (A) The internal lamination (S_0) of the psammite is marked by quartz bands, which are cross-cut by a spaced cleavage (S_1). (B) Contrasting internal bedding of two adjacent quartzitic sandstone layers, with the quartzitic sandstone on the left having a planar lamination, while the quartzitic sandstone bed on the right is characterised by a cross-lamination. The cross-lamination indicates an inverse stratigraphic polarity. (C) Mosaic breccia of the quartzitic host rock, with internal laminations showing that the brecciated fragments have maintained their initial orientation. Tape measure for scale.

bedding-cleavage intersection lineation (Fig. 17E) no conclusions can be drawn for exposure D with respect to the (non-)axial planar nature of the cleavage.

Interpretation

The extreme contrast in folding between the psammite and the quartzitic layers is related to a different way of strain accommodation. Because of their contrasting deformation style, detachment of both lithologies due to disharmonic folding occurred. While strain in the quartzitic layers was fully accommodated by intense folding (up to an isoclinal geometry), the psammite accommodated strain through the development of a spaced cleavage (Fig. 18A). As the quartzitic sandstone is very competent, it was not capable of cleavage development, and folding led to a large amount of internal strain, accommodated by faulting and fracturing. The cohesive nature of the stockwork veining, with sometimes host-rock fragments 'floating' in the vein matrix (i.e. a mosaic breccia – Fig. 18C), indicates that high, up to lithostatic, fluid pressures assisted the brittle failure of the rock (Jacques et al., 2014). The brecciated fabric of the quartzitic material, with in situ fragmented fabrics without any significant rotation of the fragments (cf. the internal bedding in the fragments that maintained their original orientation – Fig. 18C), strongly suggests fluid-assisted brecciation (e.g. Jébrak, 1997).

5. Discussion

5.1. The control of the pre-deformational context on the mixed brittle-ductile accommodation of folding

The exposures discussed illustrate different ways of accommodating folding during the main contractional stage of Variscan deformation in mixed brittle-ductile conditions. The variability in kinematic processes and subsequently the complex nature of the accommodation structures primarily originates from the pre-deformational context of the Lower Devonian metasedimentary sequence. Both the lithological heterogeneities (competence contrasts) and the sediment architecture within this sequence controlled folding and its mixed brittle-ductile accommodation by acting as buckling instabilities, nucleation points (e.g. the lenticular layer) or by influencing the nature of folding (e.g. the variable layer thickness of a point bar) (e.g. Lister & Williams, 1983).

On the one hand, the competence contrast, the thickness ratio and the spacing between different layers have directly influenced fold kinematics, as observed in exposures A and D. In exposure A, where the incompetent layer thickness is high, polyharmonic folding of the competent layers occurred (Fig. 6C-D), which was accommodated by significant hinge migration of incompetent material (Fig. 7B). Where the incompetent layer thickness was more limited, flexural slip and associated chevron-type folds with accompanying accommodation structures (e.g. boudinage and saddle reef infill) are more frequent (Fig. 8A-B). In exposure D the smaller competence contrast between the psammite and quartzite and a higher layer thickness led to disharmonic folding. While the psammite accommodated strain through the development of a spaced cleavage, the quartzite was intensely folded and subsequently fractured (Fig. 17).

On the other hand, specific sedimentary structures also influenced how the rock sequence accommodated folding. In our model for exposure B, both the nucleation of folding and its final geometry were controlled by the presence of the lenticular layer (**3**) (Fig. 13). The quartzite layer (**2**) accommodated folding in a brittle manner, with the layer in question being separated in three different fault segments (Figs 10 & 13). The overlying thick sequence of incompetent rocks, however, passively folded along the lenticular layer with the formation of a second-order fold and associated cleavage (Figs 11B & 13). In a similar fashion, the quartzitic point bar in exposure C, accommodated folding through the formation of a tectonic ramp (Figs 14A & 16), while the overlying incompetent rocks passively folded at the toe of this faulted tectonic wedge, with the formation of a second-order fold and an accompanying divergent cleavage (Figs 14A & 16).

5.2. Finite plane strain reflected in the non-cylindrical nature of fold structures

As evidenced in the study area (Fig. 2) and on a more regional scale (Fig. 5), non-cylindrical folds, with a strongly variable fold hinge attitude, typify the northwestern part of the Ardenne culmination. The non-cylindrical folds show an en-echelon configuration, with a variation from west- to east-plunging folds from north (Wellin) to south (Daverdisse), and a widely variable attitude of the fold hinges and cleavage-bedding intersection lineations. Folds are also periclinal, so that often they are not traceable on opposite sides of a river bank. Besides this regional aspect, evidence of non-cylindrical fold characteristics can also be observed within a single outcrop, e.g. the variable, double-plunging fold hinges and the slickenfibre lineations oblique to the calculated β-fold axis in exposure A (Fig. 9A-B).

We believe that these manifestations of general non-cylindrical folding indicate a finite strain deviating from pure flattening, commonly materialised by the pervasive cleavage fabric omnipresent in the HASB. In a heterogeneous rock sequence, however, a deviation from pure flattening strain can be

accommodated through non-cylindrical folding without impeding the development of a cleavage fabric (Sullivan, 2013).

Ramsay (1967) already inferred that geological structures, such as folds and boudins, record components of the finite strain. As such, depending on the orientation and magnitude of the principal strain axes, a variety of structures can develop. Constriction (X>1>Y>Z), on the one hand, gives rise to two interfering, orthogonal sets of folds, reflecting the two, mutually orthogonal, principal directions of shortening (Y and Z) perpendicular to the principal extension direction (X) (Fig. 19) (Ramsay, 1967). Flattening (X>Y>1> Z), on the other hand, is characterised by cylindrical folds with possible boudinage and cross-jointing parallel and perpendicular to the fold hinges, respectively (Fig. 19) (Ramsay, 1967). We infer, as already put forward by Treagus & Treagus (1981), that non-cylindrical folds with variably trending and plunging fold hinge lines and an en-echelon, double-plunging geometry materialise a deviation from pure flattening towards constriction. Fold hinge development oblique to the XY plane of strain, i.e. the cleavage, is more pronounced in slightly constrictional conditions and axial migration of the fold hinge towards the XY plane during progressive folding is more limited (Treagus & Treagus, 1981). Interestingly, Treagus & Treagus (1981) indicate that subparallellism of the fold hinges in en-echelon periclines is predicted for plane strain (X>Y=1>Z), while more curving and variable hinges are expected for constrictional strain (Fig. 19). As the fold hinges in the study area are still relatively subparallel to each other (they have a trend that is roughly EW-oriented – Fig. 5) and fold plunges do not exceed 20°, we infer that the finite strain in the study area approximates plane strain.

Besides these direct manifestations of non-cylindrical folding, a transecting, non axial-planar cleavage (e.g. Borradaile, 1978) was observed in some of the exposures discussed. Our model for exposure B shows that the non-axial planar cleavage developed coeval with folding, and did not originate from, or rotate in a subsequent deformation phase. We inferred that the non-axial planar cleavage in exposure B is related to first-order folding, and is overprinted locally by an axial planar cleavage, related to the development of the second-order fold along the toe of the quartzite wedge (Figs 11B & 13C). The axial planar cleavage, related to the second-order fold, excludes that the first-order non-axial planar cleavage could originate from a post-folding deformation phase. Otherwise, both cleavages would have been converted to a non-axial planar orientation. This is confirmed by the bedding girdles of the first- and second-order fold that have a consistent orientation (Fig. 12).

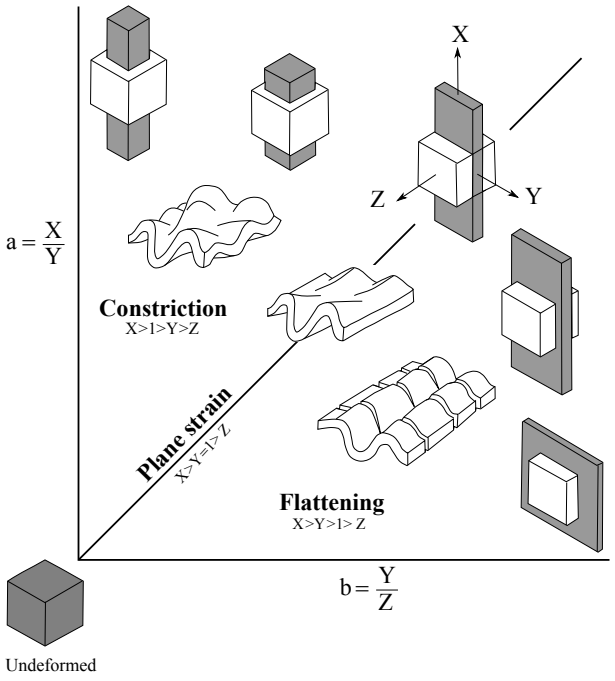

Figure 19. Flinn diagram representing three-dimensional finite strain. The shape changes of the finite strain ellipsoid are imaged together with the contractional structures that may form. Modified from Price & Cosgrove (1990).

Cleavage-transected folds have often been coupled to transpressional deformation (Debacker et al., 2004; Pratt & Fitches, 1993; Sintubin, 1999; Woodcock, 1990). The use of a transecting cleavage as a transpressional shear-sense indicator, however, although often used, is controversial as no obvious explanation exists for a transecting cleavage in simple transpression (Stringer & Treagus, 1980; Treagus & Treagus, 1992). Instead, the latter authors state that a non-axial planar cleavage results merely from fold initiation on sedimentary layering oblique to the principal strain axes. Transection angles will vary with the initial orientation (strike and dip) of the buckled layer, and will strongly increase from flattening (generally negligible angles of transection) to constrictional strain (> 10°), as non-cylindrical folding and variable bedding girdle orientations are more prominent with constrictional strain (cf. supra) (Treagus & Treagus, 1981).

We interpret, following the latter geometrical model, the local transection between the cleavage fabric and bedding as being directly related to the discussed non-cylindrical, en-echelon periclinal fold geometry. The angle and sense of cleavage transection within such a fold assemblage depends merely on the position within the fold assemblage and the fold hinge line orientation at that position. Hence, locally also apparent axial planar cleavages will be observed. The cleavage in the study area has a consistent EW-attitude. The observed non-axial planar cleavage originated thus from local complexities in the deformation, directly reflected by the variable orientation of bedding strike. The bedding girdle indeed changes from north to south in the section studied (Fig. 2A). The angular relationship between the cleavage-bedding intersection lineation and the fold axis changes accordingly from a maximum difference of 33° in exposure B (Fig. 12), to approximately 10° in exposure C (Fig. 15). Due to the large degree of scatter in the orientation measurements for exposure D, the observed offset angle of 5° will not be considered as an indication for a non-axial planar cleavage. Finally, an approximately axial-planar cleavage was observed in the northernmost part of the study area, where the cleavage-bedding intersection lineation has an orientation orthogonal to the bedding girdle. While we indicate that the amount and sense of cleavage transection is related to the variable orientation of the bedding girdle within a non-cylindrical fold train, Treagus & Treagus (1981) did argue that layers with an irregular thickness and a high initial dip reinforce the occurrence of variable fold hinge orientations and hence a strong cleavage transection. As such, the very high angle of cleavage transection in exposure B could be related to the occurrence of the lenticular quartzitic body. The remarkable absence of a non-axial planar cleavage in exposure A (Fig. 9A) can be explained by the small interlimb angle. Possibly, a non-axial planar cleavage was present in the initial stages of folding, but later bulk flattening strain in the incompetent layers likely further rotated the cleavage into near-parallelism with the axial plane of the folds (e.g. Fischer & Jackson, 1999).

5.3. Non-cylindrical folding in the regional framework of the Meuse Valley Recess transpressional corridor

The Redu-Daverdisse study area is located towards the southeastern extremity of the Meuse Valley Recess (MVR), one of the transpressional corridors in the Ardenne allochthon as defined by Lacquement et al. (2005) (Figs 20 & 21A). Within the Ardenne allochthon (France and Belgium), five transpressional zones with a general NW-SE to NS-trend are encountered (Lacquement, 2001; Mansy & Lacquement, 2002): the Ourthe zone (Dejonghe, 2008; Hance et al., 1999), the Meuse Valley Recess (Lacquement et al., 2005), the Beaumont zone, the Valenciennes zone and the Artois zone (Fig. 20). Palaeomagnetic studies (Szaniawski et al., 2003) and studies of the magnetic rock fabric (Lacquement et al., 2005; Robion et al., 1999) demonstrated vertical rotations within these corridors, accommodating dextral transpression (and sinistral in the NS-oriented Ourthe zone) during the NW-directed transport of the Ardenne allochthon on top of the pre-structured

basement (Fig. 20) (Mansy & Lacquement, 2002). Within these transpressional corridors important transport-parallel strike-slip components are accommodated in a discrete or diffuse manner, i.e. through faulting and folding, respectively. Inside the transpressional corridors, the folds have a curvilinear geometry (Lacquement, 2001), unlike the cylindrical folds outside of the corridors.

A pre-structured basement consisting of frontal ramps (dominantly ENE-WSW striking) and lateral ramps (dominantly NW-SE striking), approximately normal and parallel to the transport direction of the overriding Ardenne allochthon, respectively (Fielitz & Mansy, 1999; Mansy & Lacquement, 2002) (Fig. 20A), is considered to lie at the base of these transpressional corridors. The synsedimentary normal fault zones, active in the Ardenne-Eifel basin during early to middle Devonian rifting, have been recognised by abrupt changes in facies and stratigraphic thickness within the Ardenne allochthon (Meilliez et al., 1991).

The MVR is a 40-km wide, NW-SE oriented zone along the Meuse river valley, showing a WNW-ESE to E-W oriented structural grain that deviates from the overall NE-SW to ENE-WSW oriented structural grain within the Ardenne allochthon (Figs 5 & 21A) (Averbuch et al., 2006; Lacquement et al., 2005). This lateral change in structural grain is expressed in a variety of complex 3D fold-thrust features (Averbuch et al., 2006; Lacquement et al., 2005). Firstly, fold hinge lines show an increase in plunge (from 5 up to 50°) and a clockwise rotation of their axial trend (up to 70°) from west to east within the MVR. Secondly, the fold train in the Givet area shows an en-echelon geometry with local cleavage transection. Thirdly, the study of deep boreholes (e.g. Focant and Rosée deep wells) and seismic profiles (Raoult, 1986) demonstrated that the Givet backthrust changes in slip direction from NNW to W at the eastern boundary of the MVR (Lacquement et al., 2005). The latter reflects a component of shortening at a high angle to the regional, NNW-SSE directed, transport direction. This was also confirmed by the NNW-SSE striking magnetic fabric at the eastern boundary of the MVR, indicating a strong reworking of the tectonic foliation (Lacquement et al., 2005).

These observations reflect a buried, NW-SE striking lateral/oblique ramp in the eastern part of the MVR, with a vertical offset (up to 2 km) leading to distributed (dextral) transpressional deformation within the overlying Ardenne thrust wedge (Averbuch et al., 2006). Due to the contrasting thickness of the sedimentary sequence on both sides of the buried, oblique ramp, the Ardenne allochthon propagated differentially to the west and east of the ramp. Subsequently, drag effects and an associated component of lateral shortening occurred along the buttressing,

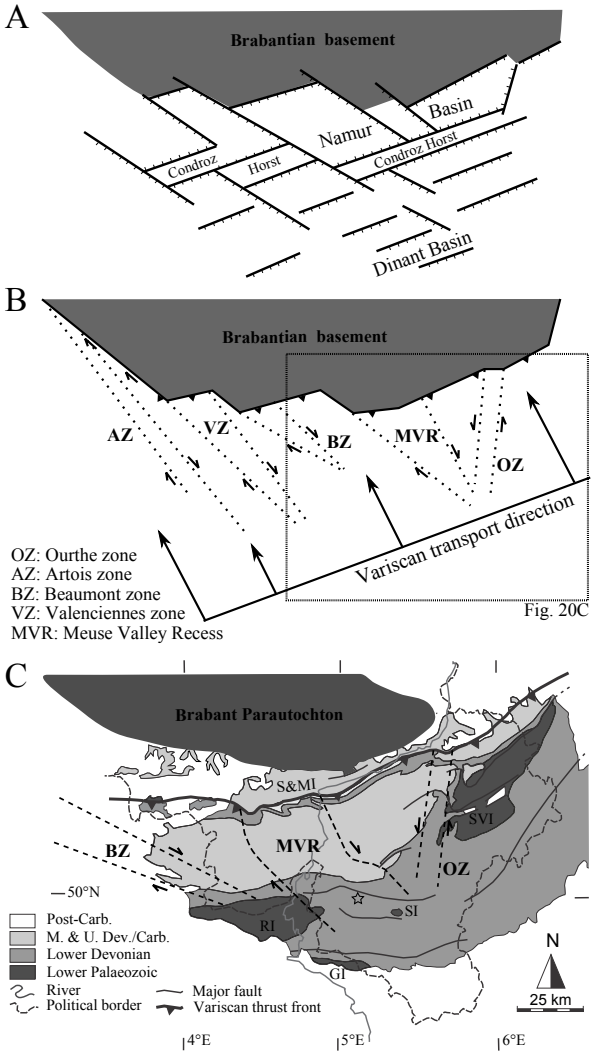

Figure 20. Model for the pre-deformational origin of the transpressional corridors in the Ardenne allochthon. Adapted after Mansy & Lacquement (2002). (A) Early to middle Devonian rifting in the Rhenohercynian basin leading to the development of ENE-WSW and NW-SE striking normal faults. (B) Upon propagation of the Variscan thrust front oblique to the Brabantian basement in the north, the ENE-WSW oriented normal faults localised transverse strike-slip fault systems. These fault systems formed corridors within the allochthonuous domain in which transpressional deformation took place. (C) Geological map of the Ardenne-Eifel area indicating the three major transpressional corridors (study area marked with a star).

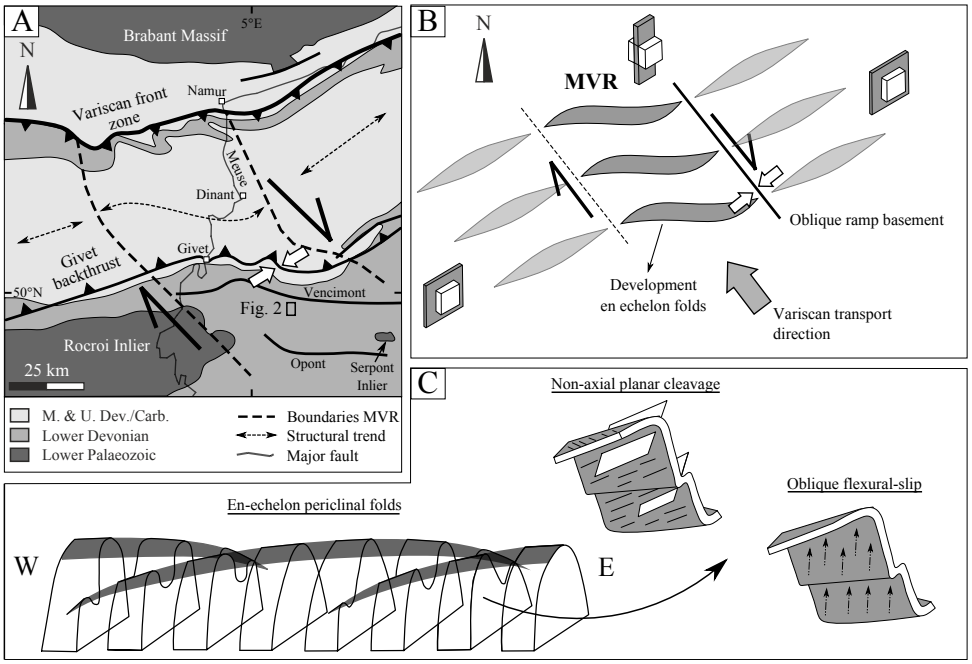

Figure 21. Conceptual model relating the transpressional setting of the Meuse Valley Recess (MVR) and the kinematics to the fold structures in the Dave-Daverdisse area. (A) Geological map outlining the MVR based on the lateral trend variation of the Variscan structural grain (after Lacquement et al., 2005). (B) Sketch of the kinematics within the MVR transpressional corridor, illustrating the rotation of the structural grain and the development of en-echelon folds due to differential propagation of the Ardenne allochthon over the buttressing, oblique ramp. Due to the resulting component of lateral contraction perpendicular to this ramp, finite strain within the MVR approximates plane strain. (C) 3D sketches of the observed en-echelon, periclinal folds that result from the transpressional kinematics (see also Fig. 19). For one section through these en-echelon folds, the related non-axial planar cleavage and oblique flexural slip are shown.

oblique ramp, leading to rotation of the structural grain along a vertical axis and inherently oblique fold development and final thrust-sheet rotation within the transpressional corridor. Hence, folds developed in an en-echelon periclinal configuration oblique to the NW-SE shortening direction (cf. kinematically simplified sketch of Fig. 21B). Because of the component of lateral shortening on top of the buttressing, oblique ramp, the finite strain within the MVR eventually approximates plane strain. This finite strain contrasts with the flattening strain observed outside of the MVR (Fig. 21B). The development of an en-echelon, periclinal fold geometry readily allows to interpret the occurrence of a non-axial planar cleavage and the oblique flexural slip (Fig. 21C). The lack of steep fold plunges and oblique thrust faults in the study area is most likely related to the more competent behaviour of the Givetian limestone, facilitating local thrust development and associated thrust sheet rotation.

In the southern part of the Dinant fold-and-thrust belt, between Han-sur-Lesse and Beauraing (approximately 10-15 km to the north of our study area), Delvaux (1989, 1997) describes the particular vergence (Z-shaped) of the Revogne fold and a series of reactivated, steeply inclined, WSW-ENE to EW-trending, transverse faults that intersect all EW-trending Variscan structures. Palaeostress tensor reconstruction of these faults infers a strike-slip to transpressional regime, with the principal horizontal compression direction oriented WNW-ESE. Minor thrusting and folding of the Revogne fold around a subvertical axis is considered to be related to this particular dextral strike-slip regime (Delvaux, 1989). Delvaux (1997) accords the inferred stress field to late Cretaceous-Cenozoic intraplate deformation that is the result of the Alpine collisional orogeny.

We believe, though, that a late Cretaceous-Cenozoic intraplate deformation, or even any deformation postdating the Variscan orogeny, cannot explain components of the non-cylindrical folding and the associated strain accommodation in our study area. In particular, the structural context of exposure B demonstrates that the first-order non-axial planar cleavage observed locally in the study area developed synchronous with the observed en-echelon, periclinal folds. Moreover, the particular Z-shaped vergence of the Revogne fold fits in the model of oblique, non-cylindrical folding above a buried lateral ramp within the transpressional setting of the MVR (Lacquement et al., 2005) (Fig. 21B).

6. Conclusions

A detailed structural analysis of a series of complex fold-related accommodation structures within a more regional context of variable fold characteristics has revealed that the finite strain in the northwestern part of the High-Ardenne slate belt (Redu-Daverdisse, Belgium) deviates from pure flattening, and approximates plane strain. Evidence stems from different manifestations of non-cylindrical folding, being en-echelon, periclinal fold geometries, mesoscale non-cylindrical folds with variable fold hinge line attitudes, oblique flexural slip and local cleavage transection. The absence of a dominant linear tectonic fabric, however, indicates that pure constriction is not yet attained. A finite strain approximating plane strain is suggested by the subparallellism of the regional EW-oriented fold hinges, without significant fold plunges.

The mesoscale, mixed brittle-ductile, fold-related accommodation structures, have a very local and complex nature. The location and geometry of these structures is strongly controlled by the original pre-deformational context. Both the lithology (i.e. competence contrasts, layer spacing and thickness) and the sediment architecture (e.g. lenticular body, point bars) of the metasedimentary sequence initiated and subsequently influenced the mixed brittle-ductile accommodation of folding. Moreover, the presence of a non-axial planar cleavage is not only dependent on the bedding girdle orientation at its position within the non-cylindrical fold geometry, but can also be reinforced by local layers with irregular thicknesses and high initial dips (e.g. the lenticular layer in exposure B, with an average transection angle of 33°).

The observed non-cylindrical fold geometry fits in the transpressional setting of the Meuse Valley Recess. This dextral transpressional corridor developed during the propagation of the Ardenne allochthonuous domain on top of a buried, oblique ramp in the pre-structured basement. Due to differential propagation to the west and east of the buttressing, oblique ramp a component of lateral shortening developed on top of the ramp with subsequently the development of oblique folding. Due to the rotation of the structural grain, non-cylindrical, en-echelon periclines and associated fold structures developed. The component of lateral shortening on top of the oblique ramp resulted in finite plane strain. Hence, we demonstrate that the Meuse Valley Recess as defined by Lacquement et al. (2005) can be continued to the SE, affecting at least the northern parts of the High-Ardenne slate belt.

7. Acknowledgments

This research is financially supported by research Grant OT/11/038 of the Onderzoeksfonds, KU Leuven, and the Agency for Innovation through Science and Technology (IWT). We greatly thank H. de Bresser and D. Delvaux for their constructive remarks that strongly improved the previous version of this article.

8. References

Aller, J., Bastida, F., Lisle, R.J. & Ramsay, J.G., 2010. Flexural slip folding of foresets in cross-bedded sandstones. Journal of Structural Geology, 32, 725-726.

Asselberghs, E., 1946. L'Eodévonien de l'Ardenne et des régions voisines. Mémoires de l'Institut géologique de l'Université de Louvain, 14, pp. 598.

Averbuch, O., Lacquement, F., Mansy, J.-L., Szaniawski, R. & Lewandowski, M., 2006. Déformations au front septentrional de la chaîne varisque: l'exemple des Ardennes franco-belges dans la région de Givet. Géologie de la France, 1-2, 85-90.

Beugnies, A., 1985. Structure de l'aire anticlinale de l'Ardenne entre les méridiens de Bertrix et de Mohret. Annales de la Société Géologique du Nord, 106, 87-95.

Beugnies, A., 1986. Le métamorphisme de l'aire anticlinale de l'Ardenne. Hercynica, 2, 17-33.

Bobillo-Ares, N.C., Bastida, F., Aller, J. & Lisle, R.J., 2009. An approach to folding kinematics from the analysis of folded oblique surfaces. Journal of Structural Geology, 31, 842-852.

Borradaile, G.J., 1978. Transected folds: a study illustrated with examples from Canada and Scotland. Bulletin of the Geological Society of America, 89, 481-493.

Bultynck, P. & Dejonghe, L., 2001. Devonian lithostratigraphic units (Belgium). Geologica Belgica, 4, 39-69.

Debacker, T. N., Sintubin, M. & Verniers, J., 2004. Transitional geometries between gently plunging and steeply plunging folds: an example from the Lower Palaeozoic Brabant Massif, Anglo-Brabant deformation belt, Belgium. Journal of the Geological Society, London, 161, 641-652.

Debacker, T.N., Dewaele, S., Sintubin, M., Verniers, J., Muchez, Ph. & Boven, A., 2005. Timing and duration of the progressive deformation of the Brabant Massif, Belgium. Geologica Belgica, 8, 20-34.

Dejonghe, L., 2008. Le couloir de décrochement dextre de l'Ourthe dans l'axe Erezée – Saint-Hubert (Haute Ardenne, Belgique) et son implication sur le tracé des failles longitudinales. Geologica Belgica, 11/3-4, 151-165.

Delvaux, D., 1989. Structures tardi- et post-Hercyniennes dans le bord sud du Synclinorium de Dinant, entre Han-sur-Lesse et Beauraing (Belgique). Annales de la Société Géologique de Belgique, 112, 317-325.

Delvaux, D., 1997. Post-Variscan right-lateral wrench faulting in the Ardenne allochton and the Variscan Front (Belgium). Aardkundige mededelingen, 8, 57-60.

Fielitz, W. & Mansy, J.-L., 1999. Pre- and synorogenic burial metamorphism in the Ardenne and neighbouring areas (Rhenohercynian zone, central European Variscides). Tectonophysics, 309, 227-256.

Fischer, M.P. & Jackson, P.B., 1999. Stratigraphic controls on deformation patterns in fault-related folds: a detachment fold example from the Sierra Madre Oriental, northeast Mexico. Journal of Structural Geology, 21, 613-633.

Fourmarier, P., 1966. Remarques à propos de petits plis en chevron et de leur signification en tectogénèse. Annales de la Société Géologique de Belgique, 67, B29-B36.

Fowler, T.J., 1996. Flexural-slip generated bedding-parallel veins from central Victoria, Australia. Journal of Structural Geology, 18, 1399-1415.

Grohmann, C.H. & Campanha, G.A.C., 2010. OpenStereo: open source, cross-platform software for structural geology analysis. Presented at the AGU 2010 Fall Meeting, San Francisco, CA.

Hance, L., Ghysel, P., Laloux, M., Dejonghe, L. & Mansy, J.-L., 1999. Influence of a heterogeneous lithostructural layering on orogenic deformation of the Variscan Front Zone (eastern Belgium). Tectonophysics, 309, 161-177.

Hudleston, P.J. & Treagus, S.H., 2010. Information from folds: A review. Journal of Structural Geology, 32, 2042-2071.

Jacques, D., Derez, T., Muchez, P. & Sintubin, M., 2014. Syn- to late-orogenic quartz veins marking a retrograde deformation path in a slate belt: Examples from the High-Ardenne slate belt (Belgium). Journal of Structural Geology, 58, 43-58.

Jébrak, M., 1997. Hydrothermal breccias in vein-type ore deposits: A review of mechanisms, morphology and size distribution. Ore Geology Reviews, 12, 111-134.

Johnson, T.E. & Woodcock, N.H., 1991. Detecting cleavage-transected folds using cleavage-bedding intersections. Journal of Structural Geology, 13, 919-925.

Jongmans, D. & Cosgrove, J. W., 1993. Observations structurales dans la région de Bastogne. Annales de la Société géologique de Belgique, 116, 129-136.

Kenis, I. & Sintubin, M., 2007. About boudins and mullions in the Ardenne-Eifel area (Belgium, Germany). Geologica Belgica, 10, 79-91.

Lacquement, F., 2001. L'Ardenne Varisque. Déformation progressive d'un prisme sédimentaire pré-structureé, de l'affleurement au modèle de chaîne. Société Géologique du Nord, 26, Lille.

Lacquement, F., Averbuch, O., Mansy, J.-L., Szaniawski, R. & Lewandowski, M., 2005. Transpressional deformations at lateral boundaries of propagating thrust-sheets: the example of the Meuse Valley Recess within the Ardennes Variscan fold-and-thrust belt (N France - S Belgium). Journal of Structural Geology, 27, 1788-1802.

Lambert, A. & Bellière, J., 1976. Caractères structuraux de l'éodévonien aux environs de Bastogne. Annales de la Société Géologique de Belgique, 99, 283-297.

Lisle, R.J., Toimil, N., Aller, J., Bobillo-Ares, N. & Bastida, F., 2010. The hinge lines of non-cylindrical folds. Journal of Structural Geology, 32, 166-171.

Lister, G.S. & Williams, P.F., 1983. The partitioning of deformation in flowing rock masses. Tectonophysics, 92, 1-33.

Mansy, J.-L. & Lacquement, F., 2002. Le Paléozoïque du Nord de la France et de la Belgique. Géologues, Revue officielle de l'Union Française des Géologues, 133-134, 7-24.

Meilliez, F., et al., 1991. Ardenne-Brabant. Sciences Géologiques Bulletin, 44, 3-29.

Meilliez, F. & Mansy, J.-L., 1990. Déformation pelliculaire différenciée dans une série lithologique hétérogène: le Dévono-Carbonifère de l'Ardenne. Bulletin de la Société géologique de France, 6, 177-188.

Oncken, O., von Winterfeld, C.H. & Dittmar, U., 1999. Accretion of a rifted passive margin: The Late Paleozoic Rhenohercynian fold and thrust belt (Middle European Variscides). Tectonics, 18, 75-91.

Picqué, A., Huon, S. & Clauer, N., 1984. La schistosité hercynienne et le métamorphisme associé dans la Vallée de la Meuse entre Charleville-Mézières et Namur (Ardennes franco-belges). Bulletin de la Société Belge de Géologie, 93, 55-70.

Piessens, K. & Sintubin, M., 1997. Partitioning of Variscan strain in the southern part of the Caledonian Stavelot-Venn Inlier in the Ardenne Allochthon (Belgium). Aardkundige Mededelingen, 8, 135-138.

Pratt, W.T. & Fitches, W.R., 1993. Transected folds from the western part of the Bala Lineament, Wales. Journal of Structural Geology, 15, 55-68.

Price, N.J. & Cosgrove, J.W., 1990. Analysis of geological structures. University Press, Cambridge.

Ramsay, J.G., 1961. The effects of folding upon the orientation of sedimentation structures. The Journal of Geology, 69, 84-100.

Ramsay, J.G., 1967. Folding and Fracturing of Rocks. McGraw Hill, New York.

Ramsay, J.G., 1974. Development of chevron folds. Bulletin of the Geological Society of America, 85, 1741-1754.

Raoult, J.-F., 1986. Le front varisque du Nord de la France d'après les profils sismiques, la géologie de surface et les sondages. Revue de géologie dynamique et de géographie physique, 27, 247-288.

Reading, H.G., 1996. Sedimentary Environments: Processes, Facies and Stratigraphy. Blackwell Publishing, Oxford.

Robion, P., Averbuch, O. & Sintubin, M., 1999. Fabric development and metamorphic evolution of the lower Palaeozoic slaty rocks from the Rocroi Massif (French-Belgian Ardennes): new constraints from magnetic fabrics, phyllosilicate preferred orientation and illite crystallinity data. Tectonophysics, 309, 257-273.

Rondeel, H.E., 1971. About three sets of of kink bands near Herbeumont (Belgian Ardennes). Geologische Rundschau, 60, 912-923.

Schavemaker, Y.A., De Bresser, J.H.P., Van Baelen, H. & Sintubin, M., 2012. Geometry and kinematics of the low-grade metamorphic 'Herbeumont shear zone' in the High-Ardenne slate belt (Belgium). Geologica Belgica, 15, 126-136.

Sintubin, M., 1999. Arcuate fold and cleavage patterns in the southeastern part of the Anglo-Brabant Fold Belt (Belgium): tectonic implications. Tectonophysics, 309, 81-97.

Sintubin, M., Debacker, T.N. & Van Baelen, H., 2009. Early Palaeozoic orogenic events north of the Rheic suture (Brabant, Ardenne): A review. Comptes Rendues Geosciences, 341, 156-173.

Stets, J. & Schäfer, A., 2009. The Siegenian delta: land-sea transitions at the northern margin of the Rhenohercynian Basin. In: Königshof, P. (Ed.), Devonian Change: Case Studies in Palaeogeography and Palaeoecology. Geological Society, London, Special Publications, 314, 37-72.

Stringer, P. & Treagus, J.E., 1980. Non-axial planar S1 cleavage in the Hawick Rocks of the Galloway area, Southern Uplands, Scotland. Journal of Structural Geology, 2, 317-331.

Sullivan, W. A., 2013. L tectonites. Journal of Structural Geology, 50, 161-175.

Szaniawski, R., Lewandowski, M., Mansy, J.-L., Averbuch, O. & Lacquement, F., 2003. Syn-folding remagnetization events in the French-Belgium Variscan thrust front as markers of the fold-and-thrust belt kinematics. Bulletin de la Société Géologique de France, 174, 511-523.

Tanner, G.P.W., 1989. The flexural-slip mechanism. Journal of Structural Geology, 11, 635-655.

Treagus, J.E. & Treagus, S.H., 1981. Folds and the strain ellipsoid: a general model. Journal of Structural Geology, 3, 1-17.

Treagus, S.H. & Treagus, J.E., 1992. Transected folds and transpression: how are they associated? Journal of Structural Geology, 14, 361-367.

Twiss, R.J. & Moores, E.M., 1992. Structural Geology. W.H. Freeman and Company, New York.

Urai, J.L., Spaeth, G., van der Zee, W. & Hilgers, C., 2001. Evolution of mullion (formerly boudin) structures in the Variscan of the Ardennes and Eifel. Journal of the Virtual Explorer, 3, 1-15.

Van Baelen, H., 2010. Dynamics of a progressive vein development during the late-orogenic mixed brittle-ductile destabilisation of a slate belt. Examples of the High-Ardenne slate belt (Herbeumont, Belgium). Aardkundige Mededelingen, 24, Leuven University Press.

van der Pluijm, B.A. & Marshak, S., 1997. Earth Structure. An introduction to structural geology and tectonics. WCB/McGraw-Hill.

Williams, P.F., 1979. The development of folds in a cross-laminated siltstone. Journal of Structural Geology, 1, 19-30.

Woodcock, N.H., 1977. Specification of fabric shapes using an eigenvalue method. Bulletin of the Geological Society of America, 88, 1231-1236.

Woodcock, N.H., 1990. Transpressive Acadian deformation across the Central Wales Lineament. Journal of Structural Geology, 12, 329-337.

Manuscript received 10.07.2013, accepted in revised form 24.05.2014, available on line 15.06.2014